Chem

Article

Single-molecule spectroscopic probing of N-heterocyclic carbenes on a two-dimensional metal

Graphical abstract

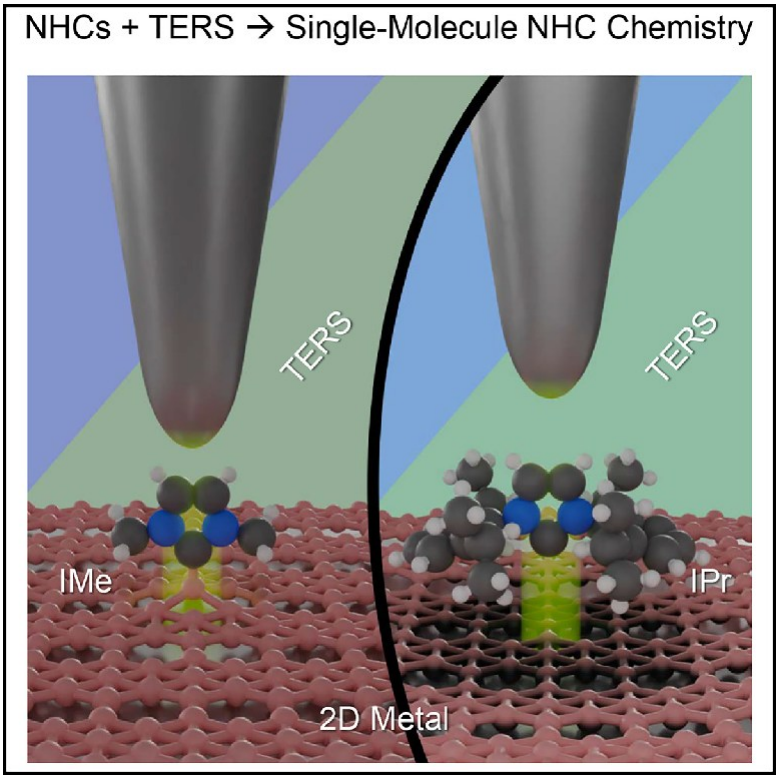

Highlights

- N-heterocyclic carbenes (NHCs) are used to modify a two-dimensional metal
- The first tip-enhanced Raman spectroscopy measurements of NHCs are reported
- Individual NHC-modified local work functions of metal surfaces are determined
- This study opens up an avenue for investigating single-molecule NHC chemistry

Authors

Linfei Li, Sayantan Mahapatra, Jeremy F. Schultz, Xu Zhang, Nan Jiang

Correspondence

njiang@uic.edu

In brief

We report the use of N-heterocyclic carbenes (NHCs) to modify a two-dimensional (2D) metal, monolayer boron (i.e., borophene). Single-molecule optical and electronic spectra allow us to understand how individual NHCs interact with borophene and its impact on the structural and electronic properties of borophene. In addition to expanding the scope of NHC modifications to 2D metals, this work establishes a methodology using combined nanospectroscopies to investigate NHC surface chemistry and related applications in catalysis and nanotechnology at the single-molecule level.

Li et al., 2025, Chem *11*, 1–9
January 9, 2025
https://doi.org/10.1016/j.chempr.2024.08.013

CellPress

Please cite this article in press as: Li et al., Single-molecule spectroscopic probing of N-heterocyclic carbenes on a two-dimensional metal, Chem (2024), https://doi.org/10.1016/j.chempr.2024.08.013

Chem

CellPress

Article

Single-molecule spectroscopic probing of N-heterocyclic carbenes on a two-dimensional metal

Linfei Li,[1] Sayantan Mahapatra,[1] Jeremy F. Schultz,[1] Xu Zhang,[2] and Nan Jiang[1,3,4,*]
[1]Department of Chemistry, University of Illinois Chicago, Chicago, IL 60607, USA
[2]Department of Physics and Astronomy, California State University, Northridge, Northridge, CA 91330, USA
[3]Department of Physics, University of Illinois Chicago, Chicago, IL 60607, USA
[4]Lead contact
*Correspondence: njiang@uic.edu
https://doi.org/10.1016/j.chempr.2024.08.013

THE BIGGER PICTURE Single-molecule insight into the nature of ligand binding to metals forms the foundation for harnessing organic modification for a variety of energy and nanoelectronic applications. Here, we use advanced nanospectroscopic methods to study the modification of a two-dimensional metal via N-heterocyclic carbenes (NHCs). We are able to generate sub-nanometer-resolved optical and electronic spectra to determine the chemical fingerprint, adsorption configuration, interfacial interaction, and local work function information of individual NHCs. This work paves the way for investigating single-molecule NHC chemistry, which is critical to understanding and controlling the fundamental properties and functions of NHC-modified materials. Significantly, we establish combined single-molecule optical/electronic spectroscopies as a promising methodology to study surface modification at the spatial limit.

SUMMARY

N-heterocyclic carbenes (NHCs) have recently proven to be powerful ligands for planar surface modification in terms of chemical and electronic properties due to their structural diversity, property tunability, and high affinity for a diverse array of elements. However, the utilization of NHCs for planar surface modification has almost exclusively been limited to bulk substrates. Here, we investigate the adsorption of NHCs on a two-dimensional (2D) metal (i.e., borophene) using combined single-molecule optical/electronic spectroscopy. Tip-enhanced Raman spectroscopy reveals two distinct interfacial states between individual NHCs and borophene, which correspond to covalent (boron–carbon bonding) and van-der-Waals-type interactions. Furthermore, the impact of NHC modification on borophene's electronic properties is demonstrated by local work function reductions, as measured by scanning tunneling spectroscopy. In addition to providing novel insight into NHC–substrate interactions in the 2D regime, this study opens up an avenue for investigations of single-molecule NHC chemistry.

INTRODUCTION

The discovery of the first isolated and stable N-heterocyclic carbene (NHC) initiated intensive research on this class of ligands along with an explosive increase in their utilization across multiple fields of academia and industry.[1,2] The extensive interest arises from the well-established high affinity of NHCs toward various metal species (from nanoscale to bulk) and their superior stability compared with other reagents (e.g., thiols).[3,4] Recently, NHCs have found new applications in surface chemistry, serving as molecular modifiers for planar surfaces.[5–13] Due to their high structural modularity and functional versatility, NHCs promise to impart tailored chemical reactivity and electronic properties to planar surfaces for applications in heterogeneous catalysis and nanoelectronics.[14,15]

Thus far, NHC-modified planar surfaces have primarily been studied in the context of bulk materials (e.g., transition metals, semiconductors, and metal oxides).[16–18] As one of the most investigated classes of materials, two-dimensional (2D) materials show unique structures and exotic properties distinct from those of their bulk counterparts. Nonetheless, little attention has been devoted to the NHC modification of 2D materials despite its promise for realizing the full potential of 2D materials.[19,20] As a 2D metal, monolayer boron (i.e., borophene) has been realized recently with intriguing physical and chemical properties.[21,22] In particular, borophene boasts extraordinary flexibility and thus high responsiveness due to its atomic thinness and the unique nature of boron–boron bonds,[23] which makes it an ideal platform to investigate delicate interfacial interactions with molecules.[24] Significantly, the study of the

Please cite this article in press as: Li et al., Single-molecule spectroscopic probing of N-heterocyclic carbenes on a two-dimensional metal, Chem (2024), https://doi.org/10.1016/j.chempr.2024.08.013

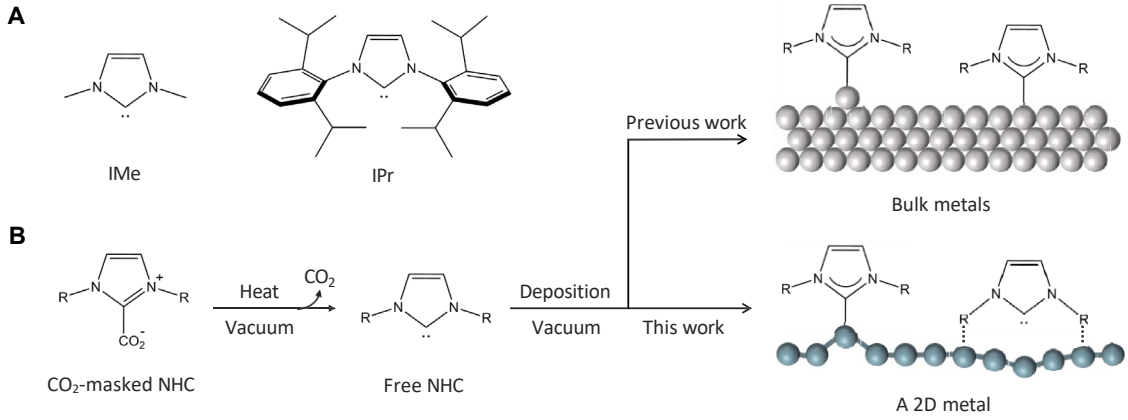

Figure 1. NHC adsorption on metals

(A) NHCs used in this work.

(B) Established recipe of vacuum deposition of NHCs on metal surfaces. NHC adsorption on bulk metals has been extensively investigated; by contrast, the interaction between NHCs and 2D metals, as studied in this work, is yet to be explored.

adsorption of NHCs on borophene could provide new insight into the interaction of NHCs with metals.

On the other hand, we believe that investigating NHCs on the single-molecule level will promote in-depth understandings of their intrinsic properties by revealing microscopic behaviors and mechanisms that are otherwise obscured in ensemble-averaging measurements. Despite their importance, single-molecule studies of NHCs remain largely unexplored due to the demand for ultrahigh chemical/energy spatial resolution. One promising approach to address this challenge is to use single-molecule optical/electronic spectroscopy, such as tip-enhanced Raman spectroscopy (TERS) and scanning tunneling spectroscopy (STS). In particular, TERS couples the chemical specificity of Raman spectroscopy with the spatial resolution of scanning tunneling microscopy (STM),[25–27] enabling the chemical interrogation of single molecules and their interactions with local nanoenvironments.[24,28–34] Combined with single-molecule STS measurements, TERS promises to provide a paradigm for single-molecule studies of NHCs.

RESULTS AND DISCUSSION

Herein, we present a single-molecule spectroscopic study of NHCs on borophene using combined TERS, STM, STS, and density functional theory (DFT). For comparative analysis, two archetypal NHC molecules, 1,3-dimethylimidazol-2-ylidene (IMe) and 1,3-bis(2,6-diisopropylphenyl)imidazol-2-ylidene (IPr), were used to tune the NHC–borophene interaction (Figure 1A). Borophene is composed of a monolayer triangular boron lattice modified by periodic networks of hollow hexagons.[35,36] Electronically, borophene is demonstrated to be metallic,[21,22] establishing it as the lightest 2D metal. In this study, we employed one of the polymorphs of borophene (i.e., $v_{1/6}$ phase, Figure S1) as the substrate for NHC growth,[22,24,35] which was prepared by electron-beam evaporation of boron atoms from a boron rod onto Ag(111) surfaces (see methods).[21,22] Notably, the STM topography of borophene is bias-dependent (Figure S1), meaning single layers of borophene can be imaged as islands or depressions with respect to Ag surfaces depending on the applied sample biases.[32]

Growth and characterization of IMe on borophene

Following the established recipe of ultrahigh vacuum (UHV) deposition of NHCs (Figure 1B),[8,12,17] we removed the $–CO_2$ mask groups of IMe–CO_2 adducts by UHV heating and then deposited the resultant free IMe onto borophene. In particular, the substrate was kept at a low temperature during molecular deposition to allow for the formation of isolated single molecules on the surface (see methods). Figure 2A shows a borophene island on Ag(111) following low-coverage IMe deposition. In addition to the Ag(111) surface (Figure S2A), isolated IMe molecules are observed to adsorb onto the terrace and edge of the borophene island. Individual IMe molecules on borophene appear as round protrusions, implying free molecular rotation around an axis perpendicular to the borophene plane.[8] At high coverages, local stripe-like molecular arrangements are present (Figure S3), although no large-scale self-assembled monolayers are observed, suggesting the relatively low mobility of IMe on borophene.

As shown in Figure 2B, the energetically favorable structure established in DFT modeling reveals an upright adsorption of IMe on borophene. Remarkably, the adsorption of IMe lifts a borophene boron atom from its crystallographic position by a height of 1.0 Å. Consequently, a single B–C bond is proposed between the lifted boron atom and the carbene carbon atom, which accounts for the free molecular rotation. The covalent binding nature of IMe on borophene is additionally supported by the extraordinarily high thermal stability of IMe–B complexes up to at least 300°C (Figure S4). Notably, NHC adsorption on gold substrates generally leads to the formation of Au adatoms and resulting NHC–Au adatom complexes on the surface,[6,8,10] which is responsible for the high surface mobility of NHCs. In contrast to this scenario, the strong covalent bonds between boron atoms in borophene prevent the IMe-bonded boron atom from

Please cite this article in press as: Li et al., Single-molecule spectroscopic probing of N-heterocyclic carbenes on a two-dimensional metal, Chem (2024), https://doi.org/10.1016/j.chempr.2024.08.013

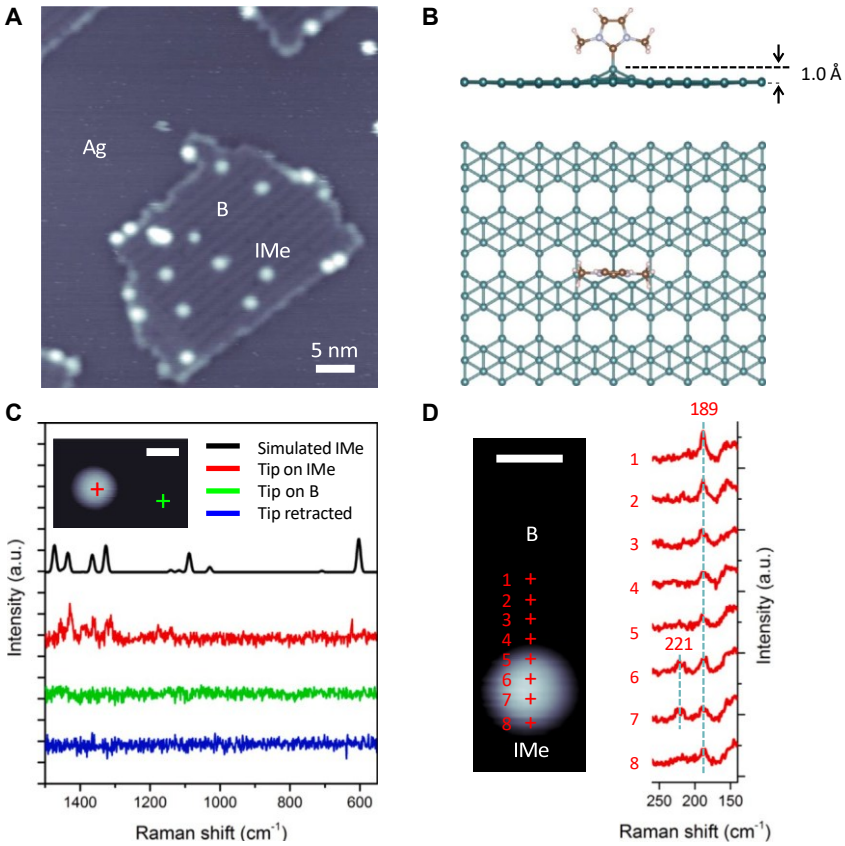

Figure 2. IMe adsorption on borophene

(A) STM image of single IMe molecules on borophene supported on Ag(111).

(B) Optimized adsorption geometry of IMe on borophene in side and top views.

(C) TERS spectra measured above a single IMe (red) and bare borophene (green). The simulated Raman spectrum of an IMe on borophene (black) is presented for comparison. Scale bar: 1 nm.

(D) TERS spectra consecutively collected along the line trace indicated in the STM image. Scale bar: 1 nm.

STM conditions: (A) 3.5 V, 30 pA; (C) 1.0 V, 15 pA; (D) 1.0 V, 30 pA.

TERS parameters: (C) 0.1 V, 1.0 nA, 5 s. (D) 0.6 V, 0.7 nA, 5 s, with a step length of 3.0 Å.

being pulled laterally out of borophene, i.e., forming an adatom on the surface. As a result, "free" IMe–B adatom complexes are absent therein, which is consistent with the observed poor mobility of IMe on borophene.

To substantiate the above theoretical analyses, TERS was employed to probe the interaction between IMe and borophene. The schematic TERS setup used in this study is illustrated in Figure S5. Specifically, the Raman scattering of a molecule underneath the STM tip can be significantly enhanced by a highly localized and intense enhanced electromagnetic field ("hot spot"), which is generated by local surface plasmon resonances at the Ag tip's apex under laser illumination. In contrast to STM, which is ideally suited for investigations of planar molecules, the ability of TERS to obtain spatially resolved vibrational information particularly excels in addressing supported nonplanar structures and tilted (or upright) geometries,[37–41] e.g., classical NHC–metal complexes. Significantly, the sub-nanometer spatial resolution of TERS makes it possible to quantitatively probe many fundamental chemical properties at the single-molecule level.[24,32,41–44]

As shown in Figure 2C, a featureless spectrum is acquired when the tip is retracted from the substrate (blue) or parked on the bare borophene surface (green), indicating the cleanliness of the tip for TERS measurements. By contrast, a distinct spectral profile (red) is observed upon placing the tip on top of the isolated molecule (see additional spectra in Figure S6), which arises from multiple molecular Raman modes. Raman simulations were then carried out based on the optimized adsorption geometry of IMe on borophene. Overall, the calculated Raman spectrum (Figure 2C, black) reproduces the measured Raman profile well (see detailed analysis in Figure S7). The small mismatch could stem from the fact that our simulation was based on a free-standing borophene without considering the strong charge-transfer interaction between borophene and Ag(111),[45] which would have an influence on the Raman modes of IMe covalently grafted on borophene. Significantly, the agreement between the theoretical simulation and experimental observation validates the adsorption configuration shown in Figure 2B.

Furthermore, to gain insight into the impact of IMe adsorption on the structural properties of borophene, we present Raman spectra consecutively acquired along a line trace across the interface between an IMe and borophene (Figure 2D). Two important observations can be made. First, the 189 cm^{-1} peak, which has been assigned to the characteristic Raman mode (B^2_{3g}) of pristine $v_{1/6}$ borophene (Figure S8A),[24,32,46] is consistent across the molecular interface, suggesting that the adsorption of IMe does not lead to a detectable phonon shift of borophene. Second, a new peak located at 221 cm^{-1} is observed on the IMe-adsorbed borophene area (positions 6 and 7), along with a low-energy peak at 189 cm^{-1} that appears consistent with those of the pristine borophene shown in positions 1–5.

To elucidate these observations, Raman simulations of IMe-modified borophene were carried out. It was found that IMe-induced local buckling of the borophene lattice gives rise to two new phonon modes located at 185 and 217 cm^{-1}, which agree excellently with the observed Raman peaks (189 and 221 cm^{-1}) on IMe-adsorbed borophene. As illustrated in Figures S8B and S8C, these two phonon modes correspond to predominantly vertical atomic displacements, in line with the surface selection rules of TERS.[47,48] In particular, the 185 cm^{-1} mode is very close in energy to the B^2_{3g} mode of pristine borophene (186 cm^{-1}, Figure S8A), which makes them hardly

Please cite this article in press as: Li et al., Single-molecule spectroscopic probing of N-heterocyclic carbenes on a two-dimensional metal, Chem (2024), https://doi.org/10.1016/j.chempr.2024.08.013

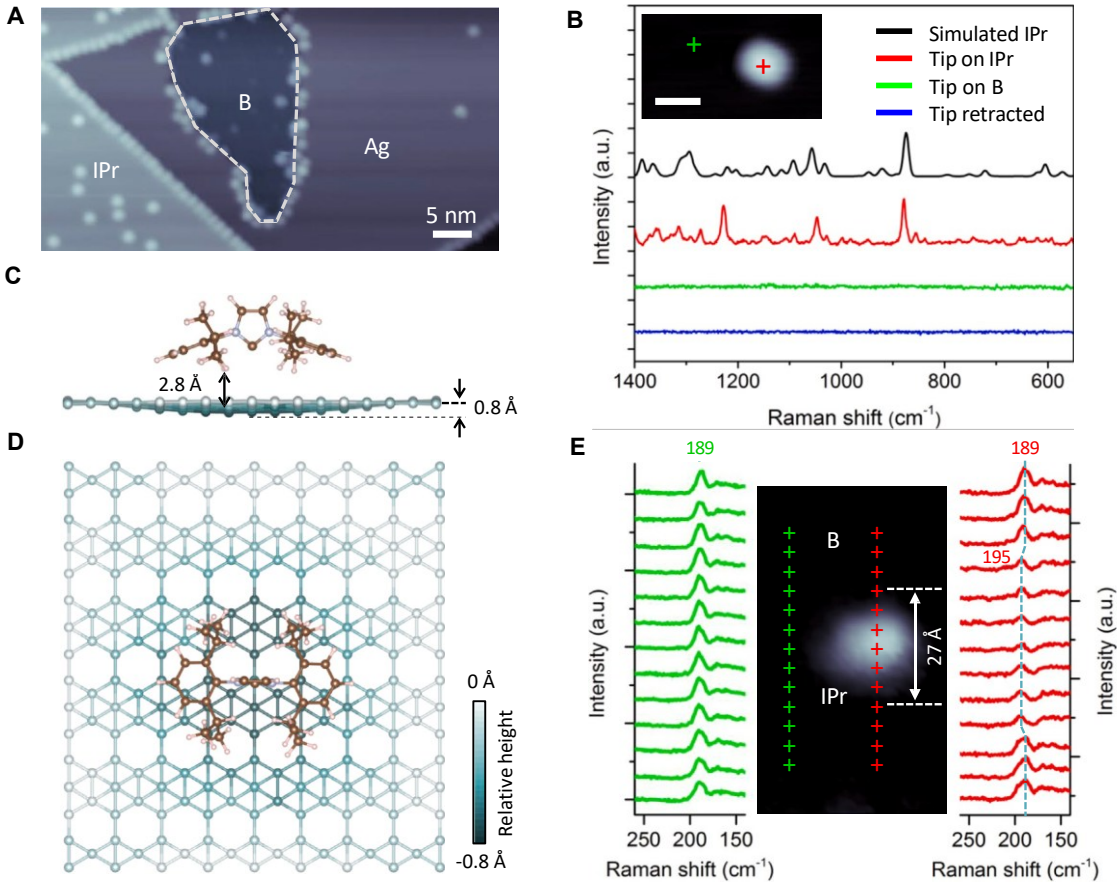

Figure 3. IPr adsorption on borophene

(A) STM image of a borophene island on Ag(111) following IPr deposition. The borophene island indicated by a dashed-line polygon is imaged as a depression.

(B) TERS spectra acquired on an isolated IPr molecule (red) and bare borophene surface (green). For comparison, the simulated Raman spectrum of an IPr on borophene (black) is also displayed. Scale bar: 2 nm.

(C and D) Side (C) and top (D) views of the energetically favorable adsorption geometry of IPr on borophene.

(E) Plots of TERS line scans along the tip traces indicated in the STM image. The red tip trace crosses an IPr molecule on borophene. Blue dashed lines are placed over TERS spectra to lead eyes.

STM conditions: (A) −1.0 V, 120 pA; (B) 1.2 V, 34 pA; (E) 3.0 V, 100 pA.

TERS parameters: (B) 0.1 V, 1.0 nA, 10 s; (E) 0.1 V, 1.5 nA, 5 s, with a step length of 4.5 A°.

distinguishable from each other, in agreement with the apparent consistency of the 189 cm^{-1} peaks in TERS profiles (Figure 2D, positions 1–8). Significantly, the most intense atomic displacements of the 217 cm^{-1} mode are highly localized underneath the IMe (Figure S8C), consistent with the observed spatially local enhancement of the 221 cm^{-1} mode at positions 6 and 7. These results demonstrate IMe-induced atomic-scale lattice variation and phonon modes of borophene, underlining the effect of NHC modification on the local structural and chemical properties of 2D materials.

Growth and characterization of IPr on borophene

To tune the NHC–borophene interaction and gain insight into the influence of NHC structures on adsorption behaviors, we next investigated the adsorption of IPr on borophene. With much larger side groups compared with IMe, IPr is expected to exhibit a different adsorption geometry and strength on borophene. As shown in Figure 3A, the Ag(111) surface is dotted with single molecules following low-coverage IPr deposition (Figure S2B). In addition, IPr molecules are observed to selectively adsorb to the edge of borophene islands (Figure S9), which is most likely attributed to the distinct electronic properties therein arising from low-coordinated boron sites. By contrast, the borophene plane is found to be inert to molecular adsorption, implying a relatively weak interaction of borophene with IPr compared with IMe. Notably, similar preferential adsorption onto metal surfaces rather than 2D materials grown on them has been predominately observed for organic molecules that feature non-bonding coupling with substrates.[24,49,50] Furthermore, the zoomed-in image illustrates that IPr on borophene appears as an elongated protrusion (Figure S10), in sharp contrast to borophene-adsorbed IMe that is imaged as a round protrusion (Figures 2C and 2D). This observation hints toward the lack of free molecular rotation and a distinct

Please cite this article in press as: Li et al., Single-molecule spectroscopic probing of N-heterocyclic carbenes on a two-dimensional metal, Chem (2024), https://doi.org/10.1016/j.chempr.2024.08.013

adsorption configuration of IPr on borophene. More IPr deposition allows for a high coverage of molecules adsorbing to borophene surfaces. Randomly distributed single molecules rather than well-ordered molecular patterns are predominant on borophene (Figure S11), indicating the ill-defined registry of IPr with borophene due to their weak interfacial interactions. The weak coupling of IPr with borophene is also supported by its poor thermal stability (Figure S12).

To chemically determine the detailed adsorption geometry of IPr that is obscured in STM images, TERS measurements were conducted. Figure 3B presents the Raman spectrum (red) acquired on a single IPr on borophene with a distinctly different spectral profile from that of IMe. Again, when the tip is moved to the molecule-free area on borophene or withdrawn from the surface, the spectral features disappear (green and blue spectra), unambiguously verifying that the TERS signal observed in the red spectrum results only from the molecule on borophene. We then performed Raman simulations based on the optimized adsorption geometry of IPr on borophene shown in Figures 3C and 3D. Notably, the simulated spectrum (Figure 3B, black) matches with the measured one nicely (see detailed analysis in Figure S13), validating the theoretically established adsorption geometry. In particular, the bulky wingtip (alkyl) groups force IPr into an upright adsorption geometry due to strong steric hindrance, where the carbene carbon is located too far from the borophene surface to directly bond to a boron atom. Instead, the borophene lattice interacts with the H atoms from the $–CH_3$ groups at a short distance, around 2.8 Å. Given that the van der Waals (vdW) radii of B and H are 1.92 and 1.10 Å, respectively,[51] such a short B$$$H distance contributes significantly to the dispersion energy and interfacial interaction strength. As a result, a notable atomic corrugation (0.8 Å) of the borophene lattice is visible (Figures 3C and 3D), which is consistent with the 2D nature and high bending flexibility of borophene.[23,24] This structural feature is in stark contrast to the one observed on IMe-modified borophene (Figure 2B), where the borophene surface in the vicinity of adsorbed IMe remains flat owing to the minimal steric repulsion from the small side groups. In addition, the interfacial vdW interaction and the absence of a single bond between IPr and borophene prevent free molecular rotation, which is consistent with the elongated shape of IPr observed in STM images (Figure S10).

To further shed light on the interfacial characteristics of IPr with borophene, we carried out TERS line scan measurements. Figure 3E displays how TERS spectra of borophene evolve across bare and IPr-adsorbed borophene surfaces with a step length of 4.5 Å. Excellently consistent spectral profiles (green) are observed along the tip trace (green) over the clean borophene area, suggesting the stability and reliability of the tip. By contrast, the 189 cm^{-1} peak of pristine borophene shifts to 195 cm^{-1} with reduced TERS intensities as the tip approaches the immediate vicinity of an IPr (red spectra). The blue shift of the monitored borophene phonon is indicative of compressive strain of the borophene lattice, which results from the dispersion interaction between IPr side groups and borophene, as demonstrated in a previous study for an organic/borophene junction.[24] Interestingly, the line profile analysis reveals that this lattice deformation occurs within ~27 Å in length around the molecule, meaning the NHC-induced strain of borophene is not localized just underneath the IPr but propagates outward beyond the molecular site, which is perfectly mirrored by the optimized geometry shown in Figure 3D. These results demonstrate that single-molecule chemical studies using TERS can not only identify individual NHCs chemically via their vibrational fingerprints but also, more significantly, probe their interaction with substrates quantitatively in virtue of the interface sensitivity and sub-nanoscale spatial resolution of TERS measurements.

In addition to borophene, we note that NHCs have been recently used to modify metal-supported graphene.[20] Particularly, the employed NHC molecule has side groups (isopropyl) larger than those of IMe but smaller than those of IPr. Interestingly, the NHC adsorbs to graphene with a strong vdW interaction and an additional weak C–C bonding interaction, apparently mixing the manners in which IMe and IPr interact with borophene. This comparative analysis indicates the complex and delicate role that the structure of side groups plays in determining the binding modes of NHCs.

LWF characterization of NHC-modified borophene

In addition to structural and chemical properties, the modification of electronic properties is central to using NHC chemistry to functionalize metal surfaces.[2–4] Here, we employed work function measurements as a sensitive diagnostic of surface modifications to provide insight into the electronic influence of NHC adsorption on borophene. Instead of ultraviolet or X-ray photoelectron spectroscopy that provides ensemble-averaged work function information,[17,52] we used STS-based field-emission resonance (FER) spectroscopy to measure local work functions (LWFs) at the single-molecule level. As illustrated in Figure 4A, when a high electric field exceeding the sample LWF is applied to the STM junction, electrons tunnel from the tip through a rounded triangular barrier (namely, Fowler-Nordheim tunneling), leading to a sequence of FERs numbered by n = 1, 2, . This resonant tunneling only occurs when the applied potential energy (eV_s) matches with the n^{th} FER. Therefore, the energies (eV_s) contain the contribution of the sample LWF (f). To a first approximation, the sample LWF can be estimated by the energy of the first FER (n = 1).

To measure and compare the LWFs of molecule-free and IMe-adsorbed borophene surfaces, we recorded d*I*/d*V* tunneling spectra at the same constant current. The spectra were collected below 6 V, as IMe tends to decompose or deform at higher biases (Figure S14). As shown in Figure 4B, two groups of peaks corresponding to FERs are observed above 4 V. Note that the peaks below 3 V are not correlated with FERs due to their insufficient energies for field emission. The spectra clearly demonstrate that the peak energies at each quantum number n on IMe-adsorbed borophene are smaller than those of pristine borophene, suggesting a reduced LWF due to NHC modification. The band shift observed on the first FER (n = 1) represents the relative variation of the work function between borophene surfaces with and without NHC modification ($Df^{Exp:}_{IMe}$ = 0.146 eV, see statistics in Figure S15), which is in excellent agreement with DFT calculations (Df^{DFT}_{IMe} = 0.144 eV, Figure S16). It is noteworthy that work functions are highly dependent on the coverage of surface

Please cite this article in press as: Li et al., Single-molecule spectroscopic probing of N-heterocyclic carbenes on a two-dimensional metal, Chem (2024), https://doi.org/10.1016/j.chempr.2024.08.013

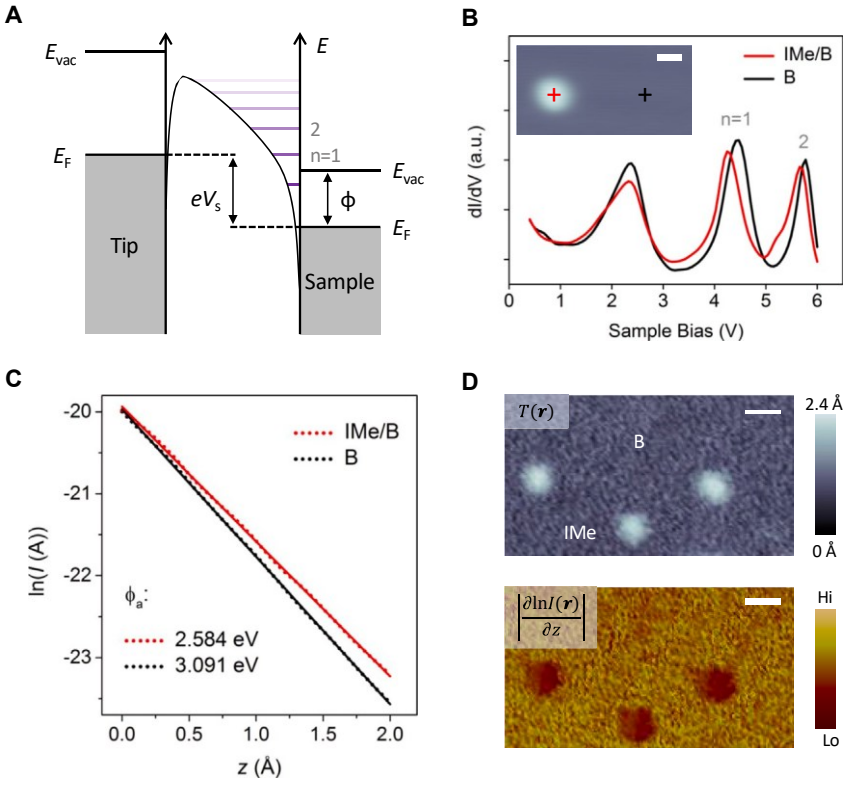

Figure 4. Local work function measurements of NHC-modified borophene

(A) Schematic energy alignment in a tip-sample junction in the field-emission resonance (FER) regime. E_{vac}, vacuum level; E_F, Fermi level; V_s, sample bias; f, sample work function; n, quantum number of FERs.

(B) FER spectra acquired on an IMe molecule and bare borophene surface, suggesting a local work function reduction of borophene due to IMe modification. Scale bar: 1 nm.

(C) Apparent barrier height (ABH, f_a) measurements of pristine and IMe-adsorbed borophene. Dots and lines represent experimental data and linear fits, respectively.

(D) Topography (top) and simultaneously acquired ABH (bottom) images of IMe-adsorbed borophene by recording the *z* derivative of the logarithm of the tunneling current *I*. Scale bars: 2 nm.

STM conditions: (B) 1.5 V, 30 pA; (D) 30 mV, 1 nA.

adsorbates.[52,53] The fact that only a single NHC molecule was involved in our measurements and calculations accounts for the small variations in LWFs, in contrast to those reported for surfaces modified by macroscopic populations of NHCs.[17,52]

To further corroborate NHC-induced LWF changes, we performed apparent barrier height (ABH) measurements that sense surface potential. Although it is hard to quantitatively relate ABHs to sample LWFs due to the dependence of ABHs on both sample and tip work functions, as well as complex barrier shapes, ABHs have been demonstrated to correlate positively with LWFs.[53–55] By modulating the tip-sample separation *z* and measuring the resultant variation of the tunneling current *I* (i.e., dln*I*/d*z*), ABHs can be determined based on the following relationship: dln*I*/d*z*f-2k, k = $(2mf_a)^{1/2}$/-, where m is the electron mass and f_a is the ABH.[56] The ABHs calculated from the slopes in Figure 4C using the equation above demonstrate that the adsorption of IMe lowers the work function of borophene, consistent with the LWF variations determined by FER measurements and DFT calculations. In particular, by recording dln*I*/d*z* during constant-current imaging, the ABHs (reflecting the relative LWFs) of pristine and IMe-modified borophene can be directly visualized. It is clearly shown in Figure 4D that the work function of borophene surface decreases in regions where IMe molecules are deposited.

Moreover, due to its distinct adsorption geometry as opposed to IMe, IPr is likely to impart different electronic properties to borophene. As illustrated in Figure S17, although a single IPr also leads to a decrease in the LWF of borophene, the reduction is considerably smaller than that caused by a single IMe, which is well supported by DFT calculations (Df_{IPr}^{DFT} = 0.080 eV, Figure S16). This result is rationalized by the minimal charge transfer and interfacial dipole between IPr and borophene due to the lack of coordination of the IPr nonbonding electron pair to the borophene surface.[52] Consistently, the dependence of work function modification on the structures of NHCs has been established for NHC-adsorbed gold and silicon surfaces.[17,52] Given the structural diversity and modularity of NHCs, the rational choice and controlled variation of NHCs is expected to provide the opportunity to tailor-make work functions.

Conclusions

With combined TERS and STM/S measurements and DFT calculations, we have revealed the interactions of model NHCs with a 2D metal at the single-molecule level. In particular, we described the critical role of side groups in determining the binding mode of NHCs, as demonstrated by the distinct interfacial characteristics of single IMe and IPr on borophene and the resultant different LWF reductions. This study expands the scope of NHC-based surface modification to the realm of 2D materials and deepens the understanding of the nature of NHC binding to metals. This novel insight into the interaction of NHCs with borophene is expected to inform future efforts aimed at modifying and functionalizing a variety of other 2D materials for energy and electronic applications. In addition, with outstanding subsurface sensitivity and sub-nanometer resolution, single-molecule optical/electronic spectroscopic characterizations depict how NHC chemistry can be investigated at the most fundamental level by probing the intrinsic properties of individual NHC molecules and their effects on local environments. This, combined with probe-based molecular manipulation, allows a prospect of understanding, tuning, and controlling NHC chemistry and, more broadly, surface chemistry at the spatial limit.

Please cite this article in press as: Li et al., Single-molecule spectroscopic probing of N-heterocyclic carbenes on a two-dimensional metal, Chem (2024), https://doi.org/10.1016/j.chempr.2024.08.013

EXPERIMENTAL PROCEDURES

Methods

Sample growth

All sample growth was performed in a commercial UHV preparation chamber (~1 × 10^{-10} torr) equipped with a standard molecular beam epitaxy setup. The Ag(111) surface was cleaned by repeated cycles of Ar^+ ion sputtering followed by annealing up to ~820 K. Borophene was prepared by electron-beam evaporation (ACME Technology) of a boron rod (99.9999% purity, ESPI Metals) onto the clean Ag(111) surface, which was held at 673 K. Borophene coverage was controlled by the duration of boron deposition using a fixed evaporation flux. Typically, a duration of 15–30 min can achieve sub-monolayer coverage. NHC molecules (>98.0% purity, Millipore-Sigma) were deposited via a standard Knudsen cell (ACME Technology) onto borophene/Ag(111) samples that were kept at low temperature. The evaporation temperature of NHC–CO_2 adducts was in the range of 315–333 K, which allows the desorption of CO_2 mask groups and thus the deposition of free NHCs on surfaces. For low-temperature deposition, the borophene sample was first cooled down to ~78 K on the STM stage (1 h) and then transferred quickly to the load-lock chamber for NHC deposition. The as-grown NHC/borophene/Ag(111) sample was immediately returned to the STM stage for characterizations. The whole transfer process typically takes 1–2 min, allowing the substrate to be kept at temperatures far lower than room temperature.

STM/S and TERS characterizations

All STM/S and TERS characterizations were carried out under 78 K using chemically etched Ag tips in a UHV variable-temperature STM system (USM1400, UNISOKU) coupled with a home-built optical setup. All STM images were obtained in constant-current mode. A 561 nm solid-state continuous-wave laser (Lasos Laser GmbH), polarized parallel to the Ag tip, was used as the excitation photon source with a laser power of 6 mW for TERS experiments. In-vacuo lenses are built inside the STM chamber and positioned in close proximity to the tip, allowing for optimal laser spot focusing and maximum collection efficiency, which is significantly beneficial to achieving single-molecule sensitivity. A detailed description of our home-built optical setup is available in our previous publications.[57,58] Specific STM and TERS measurement parameters have been included in the figure captions. To conduct FER spectroscopy, a lock-in amplifier was used to generate a 30 mV bias modulation at ~980 Hz and to obtain differential conductance while the sample bias was swept from 0.4 to 6 V with a closed (active) feedback loop. For ABH (f_a) measurements, a tiny oscillation ~0.5 Å of z-piezo was produced by the lock-in amplifier, which resulted in a modulation (dln*I*/dz) of the tunneling current *I*. Using the equation $f_a(eV) = 0.952[d\ln(A)/dz(Å)]^2$, where units are enclosed in parentheses, the ABHs of pristine and NHC-modified borophene can be determined by obtaining the slope of the linear fit of ln*I* with *z*.

Theoretical models

DFT simulations were performed to calculate the adsorption of IMe and IPr on the $v_{1/6}$ borophene, which was modeled with a supercell consisting of (10 × 6) unit cells. The DFT calculations were carried out using the VASP package[59] with the projector augmented wave pseudopotentials[60] and the Perdew-Burke-Ernzerhof generalized gradient approximation.[61] An energy cutoff of 400 eV was used for the plane-wave basis set. Only the G-point in the Brillouin zone was used considering the large size of the supercell. The van der Waals interaction was included by using a non-local correlation functional.[62,63] All atoms were fully relaxed with the force convergence criterion being 0.01 eV/Å. The phonon modes of the adsorbed IMe and IPr on borophene were obtained by solving the eigenvalue problems of a dynamical or Hessian matrix based on density functional perturbation theory calculations.[64] Time-dependent DFT calculations[65] were employed to determine the Raman intensity of adsorbed IMe and IPr molecules. The work functions were determined by the difference between the vacuum potential and the Fermi level of pristine borophene, IMe-adsorbed borophene, and IPr-adsorbed borophene.

RESOURCE AVAILABILITY

Lead contact

Further information and requests for resources should be directed to and will be fulfilled by the lead contact, Nan Jiang (njiang@uic.edu).

Materials availability

This study did not generate new, unique reagents.

Data and code availability

There is no dataset or code associated with this paper. Any additional information required to reanalyze the data reported in this paper is available from the lead contact upon request.

ACKNOWLEDGMENTS

N.J. and L.L. acknowledge support from the National Science Foundation DMR-2211474. N.J. and S.M. acknowledge support from the National Science Foundation CHE-1944796. X.Z. acknowledges support from the National Science Foundation DMR-1828019.

AUTHOR CONTRIBUTIONS

L.L. and N.J. conceived the project. L.L. conducted the experiments and data analyses. L.L. authored the manuscript in collaboration with S.M. and J.F.S. X.Z. performed theoretical calculations. N.J. supervised the project.

DECLARATION OF INTERESTS

The authors declare no competing interests.

SUPPLEMENTAL INFORMATION

Supplemental information can be found online at https://doi.org/10.1016/j.chempr.2024.08.013.

Received: March 5, 2024
Revised: June 8, 2024
Accepted: August 20, 2024
Published: September 16, 2024

REFERENCES

1. Arduengo, A.J., Harlow, R.L., and Kline, M. (1991). A Stable Crystalline Carbene. J. Am. Chem. Soc. *113*, 361–363. https://doi.org/10.1021/Ja00001a054.
2. Bellotti, P., Koy, M., Hopkinson, M.N., and Glorius, F. (2021). Recent advances in the chemistry and applications of N-heterocyclic carbenes. Nat. Rev. Chem. *5*, 711–725. https://doi.org/10.1038/s41570-021-00321-1.
3. Smith, C.A., Narouz, M.R., Lummis, P.A., Singh, I., Nazemi, A., Li, C.H., and Crudden, C.M. (2019). N-Heterocyclic Carbenes in Materials Chemistry. Chem. Rev. *119*, 4986–5056. https://doi.org/10.1021/acs.chemrev.8b00514.
4. Zhukhovitskiy, A.V., MacLeod, M.J., and Johnson, J.A. (2015). Carbene Ligands in Surface Chemistry: From Stabilization of Discrete Elemental Allotropes to Modification of Nanoscale and Bulk Substrates. Chem. Rev. *115*, 11503–11532. https://doi.org/10.1021/acs.chemrev.5b00220.
5. Weidner, T., Baio, J.E., Mundstock, A., Große, C., Karthaüser, S., Bruhn, C., and Siemeling, U. (2011). NHC-Based Self-Assembled Monolayers on Solid Gold Substrates. Aust. J. Chem. *64*, 1177–1179. https://doi.org/10.1071/CH11173.
6. Zhukhovitskiy, A.V., Mavros, M.G., Van Voorhis, T., and Johnson, J.A. (2013). Addressable Carbene Anchors for Gold Surfaces. J. Am. Chem. Soc. *135*, 7418–7421. https://doi.org/10.1021/ja401965d.
7. Crudden, C.M., Horton, J.H., Ebralidze, I.I., Zenkina, O.V., McLean, A.B., Drevniok, B., She, Z., Kraatz, H.B., Mosey, N.J., Seki, T., et al. (2014). Ultra stable self-assembled monolayers of N-heterocyclic carbenes on gold. Nat. Chem. *6*, 409–414. https://doi.org/10.1038/Nchem.1891.
8. Wang, G.Q., Rüehling, A., Amirjalayer, S., Knor, M., Ernst, J.B., Richter, C., Gao, H.J., Timmer, A., Gao, H.Y., Doltsinis, N.L., et al. (2017). Ballbot-type

motion of N-heterocyclic carbenes on gold surfaces. Nat. Chem. *9*, 152–156. https://doi.org/10.1038/Nchem.2622.

9. DeJesus, J.F., Trujillo, M.J., Camden, J.P., and Jenkins, D.M. (2018). N-Heterocyclic Carbenes as a Robust Platform for Surface-Enhanced Raman Spectroscopy. J. Am. Chem. Soc. *140*, 1247–1250. https://doi.org/10.1021/jacs.7b12779.
10. Inayeh, A., Groome, R.R.K., Singh, I., Veinot, A.J., de Lima, F.C., Miwa, R.H., Crudden, C.M., and McLean, A.B. (2021). Self-assembly of N-heterocyclic carbenes on Au(111). Nat. Commun. *12*, 4034. https://doi.org/10.1038/S41467-021-23940-0.
11. Knecht, P., Zhang, B.D., Reichert, J., Duncan, D.A., Schwarz, M., Haag, F., Ryan, P.T.P., Lee, T.L., Deimel, P.S., Feulner, P., et al. (2021). Assembly and Manipulation of a Prototypical N-Heterocyclic Carbene with a Metalloporphyrin Pedestal on a Solid Surface. J. Am. Chem. Soc. *143*, 4433–4439. https://doi.org/10.1021/jacs.1c01229.
12. Navarro, J.J., Das, M., Tosoni, S., Landwehr, F., Koy, M., Heyde, M., Pacchioni, G., Glorius, F., and Roldan Cuenya, B. (2022). Growth of N-Heterocyclic Carbene Assemblies on Cu(100) and Cu(111): From Single Molecules to Magic-Number Islands. Angew. Chem. Int. Ed. *61*, e202202127. https://doi.org/10.1002/anie.202202127.
13. Ren, J.D., Koy, M., Osthues, H., Lammers, B.S., Gutheil, C., Nyenhuis, M., Zheng, Q., Xiao, Y., Huang, L., Nalop, A., et al. (2023). On-surface synthesis of ballbot-type N-heterocyclic carbene polymers. Nat. Chem. *15*, 1737–1744. https://doi.org/10.1038/s41557-023-01310-1.
14. Koy, M., Bellotti, P., Das, M., and Glorius, F. (2021). N-Heterocyclic carbenes as tunable ligands for catalytic metal surfaces. Nat. Catal. *4*, 352–363. https://doi.org/10.1038/s41929-021-00607-z.
15. Kang, S., Byeon, S.E., and Yoon, H.J. (2021). N-Heterocyclic Carbene Anchors in Electronics Applications. Bull. Korean Chem. Soc. *42*, 712–723. https://doi.org/10.1002/bkcs.12261.
16. Jiang, L., Zhang, B.D., Me´dard, G., Seitsonen, A.P., Haag, F., Allegretti, F., Reichert, J., Kuster, B., Barth, J.V., and Papageorgiou, A.C. (2017). N-Heterocyclic carbenes on close-packed coinage metal surfaces: bis-carbene metal adatom bonding scheme of monolayer films on Au, Ag and Cu. Chem. Sci. *8*, 8301–8308. https://doi.org/10.1039/c7sc03777e.
17. Franz, M., Chandola, S., Koy, M., Zielinski, R., Aldahhak, H., Das, M., Freitag, M., Gerstmann, U., Liebig, D., Hoffmann, A.K., et al. (2021). Controlled growth of ordered monolayers of N-heterocyclic carbenes on silicon. Nat. Chem. *13*, 828–835. https://doi.org/10.1038/s41557-021-00721-2.
18. Navarro, J.J., Das, M., Tosoni, S., Landwehr, F., Bruce, J.P., Heyde, M., Pacchioni, G., Glorius, F., and Roldan Cuenya, B. (2022). Covalent Adsorption of N-Heterocyclic Carbenes on a Copper Oxide Surface. J. Am. Chem. Soc. *144*, 16267–16271. https://doi.org/10.1021/jacs.2c06335.
19. Chae, S., Le, T.H., Park, C.S., Choi, Y., Kim, S., Lee, U., Heo, E., Lee, H., Kim, Y.A., Kwon, O.S., and Yoon, H. (2020). Anomalous restoration of sp^2 hybridization in graphene functionalization. Nanoscale *12*, 13351–13359. https://doi.org/10.1039/d0nr03422c.
20. Zhang, T.C., Khomane, S.B., Singh, I., Crudden, C.M., and McBreen, P.H. (2022). Functionalization of Metal-Supported Graphene by an N-Heterocyclic Carbene. J. Phys. Chem. C *126*, 14430–14440. https://doi.org/10.1021/acs.jpcc.2c02342.
21. Mannix, A.J., Zhou, X.F., Kiraly, B., Wood, J.D., Alducin, D., Myers, B.D., Liu, X.L., Fisher, B.L., Santiago, U., Guest, J.R., et al. (2015). Synthesis of borophenes: Anisotropic, two-dimensional boron polymorphs. Science *350*, 1513–1516. https://doi.org/10.1126/science.aad1080.
22. Feng, B.J., Zhang, J., Zhong, Q., Li, W.B., Li, S., Li, H., Cheng, P., Meng, S., Chen, L., and Wu, K.H. (2016). Experimental realization of two-dimensional boron sheets. Nat. Chem. *8*, 563–568. https://doi.org/10.1038/Nchem.2491.
23. Zhang, Z.H., Yang, Y., Penev, E.S., and Yakobson, B.I. (2017). Elasticity, Flexibility, and Ideal Strength of Borophenes. Adv. Funct. Mater. *27*, 1605059. https://doi.org/10.1002/Adfm.201605059.
24. Li, L.F., Schultz, J.F., Mahapatra, S., Liu, X.L., Shaw, C., Zhang, X., Hersam, M.C., and Jiang, N. (2021). Angstrom-Scale Spectroscopic Visualization of Interfacial Interactions in an Organic/Borophene Vertical Heterostructure. J. Am. Chem. Soc. *143*, 15624–15634. https://doi.org/10.1021/jacs.1c04380.
25. Pozzi, E.A., Goubert, G., Chiang, N., Jiang, N., Chapman, C.T., McAnally, M.O., Henry, A.I., Seideman, T., Schatz, G.C., Hersam, M.C., and Van Duyne, R.P. (2017). Ultrahigh-Vacuum Tip-Enhanced Raman Spectroscopy. Chem. Rev. *117*, 4961–4982. https://doi.org/10.1021/acs.chemrev.6b00343.
26. Mahapatra, S., Li, L.F., Schultz, J.F., and Jiang, N. (2020). Tip-enhanced Raman spectroscopy: Chemical analysis with nanoscale to angstrom scale resolution. J. Chem. Phys. *153*, 010902. https://doi.org/10.1063/5.0009766.
27. Schultz, J.F., Mahapatra, S., Li, L.F., and Jiang, N. (2020). The Expanding Frontiers of Tip-Enhanced Raman Spectroscopy. Appl. Spectrosc. *74*, 1313–1340. https://doi.org/10.1177/0003702820932229.
28. Zhang, R., Zhang, Y., Dong, Z.C., Jiang, S., Zhang, C., Chen, L.G., Zhang, L., Liao, Y., Aizpurua, J., Luo, Y., et al. (2013). Chemical mapping of a single molecule by plasmon-enhanced Raman scattering. Nature *498*, 82–86. https://doi.org/10.1038/nature12151.
29. Lee, J., Crampton, K.T., Tallarida, N., and Apkarian, V.A. (2019). Visualizing vibrational normal modes of a single molecule with atomically confined light. Nature *568*, 78–82. https://doi.org/10.1038/s41586-019-1059-9.
30. Xu, J.Y., Zhu, X., Tan, S.J., Zhang, Y., Li, B., Tian, Y.Z., Shan, H., Cui, X.F., Zhao, A.D., Dong, Z.C., et al. (2021). Determining structural and chemical heterogeneities of surface species at the single-bond limit. Science *371*, 818–822. https://doi.org/10.1126/science.abd1827.
31. Jaculbia, R.B., Imada, H., Miwa, K., Iwasa, T., Takenaka, M., Yang, B., Kazuma, E., Hayazawa, N., Taketsugu, T., and Kim, Y. (2020). Single-molecule resonance Raman effect in a plasmonic nanocavity. Nat. Nanotechnol. *15*, 105–110. https://doi.org/10.1038/s41565-019-0614-8.
32. Li, L.F., Schultz, J.F., Mahapatra, S., Lu, Z.Y., Zhang, X., and Jiang, N. (2022). Chemically identifying single adatoms with single-bond sensitivity during oxidation reactions of borophene. Nat. Commun. *13*, 1796. https://doi.org/10.1038/S41467-022-29445-8.
33. Mahapatra, S., Ning, Y.Y., Schultz, J.F., Li, L.F., Zhang, J.L., and Jiang, N. (2019). Angstrom scale chemical analysis of metal supported trans- and cis-regioisomers by ultrahigh vacuum tip-enhanced raman mapping. Nano Lett. *19*, 3267–3272. https://doi.org/10.1021/acs.nanolett.9b00826.
34. Schultz, J.F., Li, L.F., Mahapatra, S., Shaw, C., Zhang, X., and Jiang, N. (2020). Defining Multiple Configurations of Rubrene on a Ag(100) Surface with 5 Å Spatial Resolution via Ultrahigh Vacuum Tip-Enhanced Raman Spectroscopy. J. Phys. Chem. C *124*, 2420–2426. https://doi.org/10.1021/acs.jpcc.9b09162.
35. Liu, X.L., Wang, L.Q., Li, S.W., Rahn, M.S., Yakobson, B.I., and Hersam, M.C. (2019). Geometric imaging of borophene polymorphs with functionalized probes. Nat. Commun. *10*, 1642. https://doi.org/10.1038/S41467-019-09686-W.
36. Liu, X.L., Zhang, Z.H., Wang, L.Q., Yakobson, B.I., and Hersam, M.C. (2018). Intermixing and periodic self-assembly of borophene line defects. Nat. Mater. *17*, 783–788. https://doi.org/10.1038/s41563-018-0134-1.
37. Zhong, J.H., Jin, X., Meng, L.Y., Wang, X., Su, H.S., Yang, Z.L., Williams, C.T., and Ren, B. (2017). Probing the electronic and catalytic properties of a bimetallic surface with 3 nm resolution. Nat. Nanotechnol. *12*, 132–136. https://doi.org/10.1038/Nnano.2016.241.
38. Cai, Z.F., Merino, J.P., Fang, W., Kumar, N., Richardson, J.O., De Feyter, S., and Zenobi, R. (2022). Molecular-Level Insights on Reactive Arrangement in On-Surface Photocatalytic Coupling Reactions Using Tip-Enhanced Raman Spectroscopy. J. Am. Chem. Soc. *144*, 538–546. https://doi.org/10.1021/jacs.1c11263.

39. Yin, H., Zheng, L.Q., Fang, W., Lai, Y.H., Porenta, N., Goubert, G., Zhang, H., Su, H.S., Ren, B., Richardson, J.O., et al. (2020). Nanometre-scale spectroscopic visualization of catalytic sites during a hydrogenation reaction on a Pd/Au bimetallic catalyst. Nat. Catal. *3*, 834–842. https://doi.org/10.1038/s41929-020-00511-y.

40. Jiang, N., Chiang, N.H., Madison, L.R., Pozzi, E.A., Wasielewski, M.R., Seideman, T., Ratner, M.A., Hersam, M.C., Schatz, G.C., and Van Duyne, R.P. (2016). Nanoscale Chemical Imaging of a Dynamic Molecular Phase Boundary with Ultrahigh Vacuum Tip-Enhanced Raman Spectroscopy. Nano Lett. *16*, 3898–3904. https://doi.org/10.1021/acs.nanolett.6b01405.

41. Wang, R.P., Yang, B., Fu, Q., Zhang, Y., Zhu, R., Dong, X.R., Zhang, Y., Wang, B., Yang, J.L., Luo, Y., et al. (2021). Raman Detection of Bond Breaking and Making of a Chemisorbed Up-Standing Single Molecule at Single-Bond Level. J. Phys. Chem. Lett. *12*, 1961–1968. https://doi.org/10.1021/acs.jpclett.1c00074.

42. Dong, X., Yang, B., Zhu, R., Wang, R., Zhang, Y., Zhang, Y., and Dong, Z. (2022). Tip-induced bond weakening, tilting, and hopping of a single CO molecule on Cu(100). Light Adv. Manuf. *3*, 52. https://doi.org/10.37188/lam.2022.052.

43. Zhu, X., Xu, J.Y., Zhang, Y., Li, B., Tian, Y.S., Wu, Y.Y., Liu, Z.W., Ma, C.X., Tan, S.J., and Wang, B. (2023). Revealing Intramolecular Isotope Effects with Chemical-Bond Precision. J. Am. Chem. Soc. *145*, 13839–13845. https://doi.org/10.1021/jacs.3c02728.

44. Li, L.F., Schultz, J.F., Mahapatra, S., Liu, X.L., Zhang, X., Hersam, M.C., and Jiang, N. (2023). Atomic-Scale Insights into the Interlayer Characteristics and Oxygen Reactivity of Bilayer Borophene. Angew. Chem. Int. Ed. *62*, e202306590. https://doi.org/10.1002/anie.202306590.

45. Liu, X.L., Wang, L.Q., Yakobson, B.I., and Hersam, M.C. (2021). Nanoscale Probing of Image-Potential States and Electron Transfer Doping in Borophene Polymorphs. Nano Lett. *21*, 1169–1174. https://doi.org/10.1021/acs.nanolett.0c04869.

46. Sheng, S.X., Wu, J.B., Cong, X., Zhong, Q., Li, W.B., Hu, W.Q., Gou, J., Cheng, P., Tan, P.H., Chen, L., and Wu, K.H. (2019). Raman Spectroscopy of Two-Dimensional Borophene Sheets. ACS Nano *13*, 4133–4139. https://doi.org/10.1021/acsnano.8b08909.

47. Moskovits, M. (1982). Surface selection rules. J. Chem. Phys. *77*, 4408–4416. https://doi.org/10.1063/1.444442.

48. Moskovits, M., and Suh, J.S. (1984). Surface selection rules for surface-enhanced Raman spectroscopy: calculations and application to the surface-enhanced Raman spectrum of phthalazine on silver. J. Phys. Chem. *88*, 5526–5530. https://doi.org/10.1021/j150667a013.

49. Liu, X.L., Wei, Z.H., Balla, I., Mannix, A.J., Guisinger, N.P., Luijten, E., and Hersam, M.C. (2017). Self-assembly of electronically abrupt borophene/organic lateral heterostructures. Sci. Adv. *3*, e1602356. https://doi.org/10.1126/sciadv.1602356.

50. Sun, X.N., and Silly, F. (2010). NaCl islands decorated with 2D or 3D 3,4,9,10-perylene-tetracarboxylic-dianhydride nanostructures. Appl. Surf. Sci. *256*, 2228–2231. https://doi.org/10.1016/j.apsusc.2009.09.079.

51. Mantina, M., Chamberlin, A.C., Valero, R., Cramer, C.J., and Truhlar, D.G. (2009). Consistent van der Waals Radii for the Whole Main Group. J. Phys. Chem. A *113*, 5806–5812. https://doi.org/10.1021/jp8111556.

52. Kim, H.K., Hyla, A.S., Winget, P., Li, H., Wyss, C.M., Jordan, A.J., Larrain, F.A., Sadighi, J.P., Fuentes-Hernandez, C., Kippelen, B., et al. (2017). Reduction of the Work Function of Gold by N-Heterocyclic Carbenes. Chem. Mater. *29*, 3403–3411. https://doi.org/10.1021/acs.chemmater.6b04213.

53. Dougherty, D.B., Maksymovych, P., Lee, J., and Yates, J.T. (2006). Local spectroscopy of image-potential-derived states: From single molecules to monolayers of benzene on Cu(111). Phys. Rev. Lett. *97*, 236806. https://doi.org/10.1103/Physrevlett.97.236806.

54. Schintke, S., and Schneider, W.D. (2004). Insulators at the ultrathin limit: electronic structure studied by scanning tunnelling microscopy and scanning tunnelling spectroscopy. J. Phys.: Condens. Matter *16*, R49–R81. https://doi.org/10.1088/0953-8984/16/4/R02.

55. Olsson, F.E., Persson, M., Repp, J., and Meyer, G. (2005). Scanning tunneling microscopy and spectroscopy of NaCl overlayers on the stepped Cu(311) surface: Experimental and theoretical study. Phys. Rev. B *71*, 075419. https://doi.org/10.1103/Physrevb.71.075419.

56. Ruggiero, C.D., Choi, T., and Gupta, J.A. (2007). Tunneling spectroscopy of ultrathin insulating films: CuN on Cu(100). Appl. Phys. Lett. *91*, 253106. https://doi.org/10.1063/1.2825595.

57. Whiteman, P.J., Schultz, J.F., Porach, Z.D., Chen, H.N., and Jiang, N. (2018). Dual Binding Configurations of Subphthalocyanine on Ag(100) Substrate Characterized by, Scanning Tunneling Microscopy, Tip-Enhanced Raman Spectroscopy, and Density Functional Theory. J. Phys. Chem. C *122*, 5489–5495. https://doi.org/10.1021/acs.jpcc.7b12068.

58. Mahapatra, S., Li, L.F., Schultz, J.F., and Jiang, N. (2021). Methods to fabricate and recycle plasmonic probes for ultrahigh vacuum scanning tunneling microscopy-based tip-enhanced Raman spectroscopy. J. Raman Spectrosc. *52*, 573–580. https://doi.org/10.1002/jrs.5951.

59. Kresse, G., and Furthmu€ller, J. (1996). Efficient iterative schemes for ab initio total-energy calculations using a plane-wave basis set. Phys. Rev. B Condens. Matter *54*, 11169–11186. https://doi.org/10.1103/PhysRevB.54.11169.

60. Blo¨chl, P.E. (1994). Projector Augmented-Wave Method. Phys. Rev. B Condens. Matter *50*, 17953–17979. https://doi.org/10.1103/PhysRevB.50.17953.

61. Perdew, J.P., Burke, K., and Ernzerhof, M. (1996). Generalized gradient approximation made simple. Phys. Rev. Lett. *77*, 3865–3868. https://doi.org/10.1103/PhysRevLett.77.3865.

62. Dion, M., Rydberg, H., Schro¨der, E., Langreth, D.C., and Lundqvist, B.I. (2004). Van der Waals density functional for general geometries. Phys. Rev. Lett. *92*, 246401. https://doi.org/10.1103/Physrevlett.92.246401.

63. Klimevs, J., Bowler, D.R., and Michaelides, A. (2011). Van der Waals density functionals applied to solids. Phys. Rev. B *83*, 195131. https://doi.org/10.1103/Physrevb.83.195131.

64. Baroni, S., de Gironcoli, S., Dal Corso, A., and Giannozzi, P. (2001). Phonons and related crystal properties from density-functional perturbation theory. Rev. Mod. Phys. *73*, 515–562. https://doi.org/10.1103/RevModPhys.73.515.

65. Zhang, X. (2018). Large-scale ab initio calculations of Raman scattering spectra within time-dependent density functional perturbation theory. J. Chem. Phys. *148*, 244103. https://doi.org/10.1063/1.5038112.

Chem, Volume *11*

Supplemental information

Single-molecule spectroscopic probing of N-heterocyclic carbenes on a two-dimensional metal

Linfei Li, Sayantan Mahapatra, Jeremy F. Schultz, Xu Zhang, and Nan Jiang

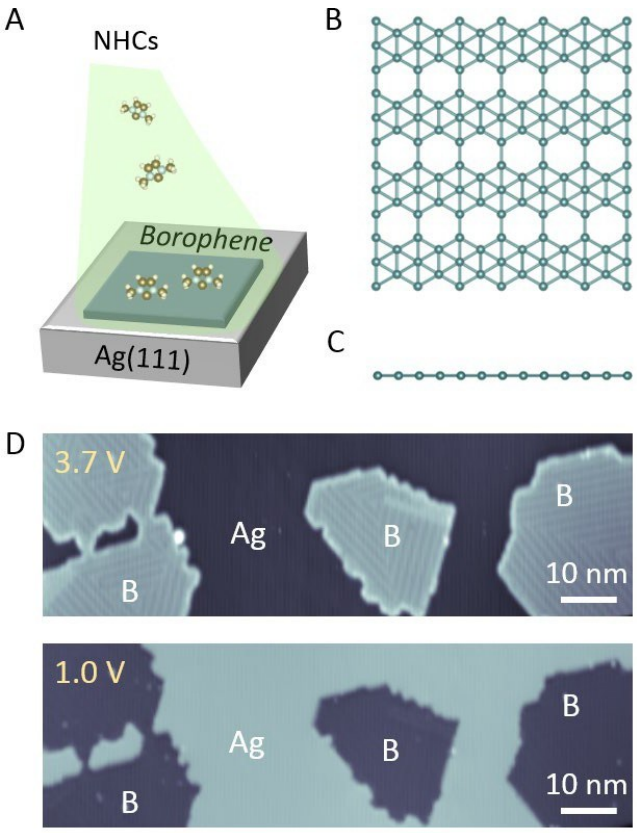

Figure S1. Atomic structure and STM topography of borophene used for NHC deposition.
(A) Schematic of NHC deposition on borophene supported on Ag(111).
(B and C) Top (B) and side (C) views of the atomic structure of $v_{1/6}$ borophene.
(D) Bias-dependent STM topography of $v_{1/6}$ borophene on Ag(111) imaged with the same tunneling current (30 pA) but different sample biases as indicated.

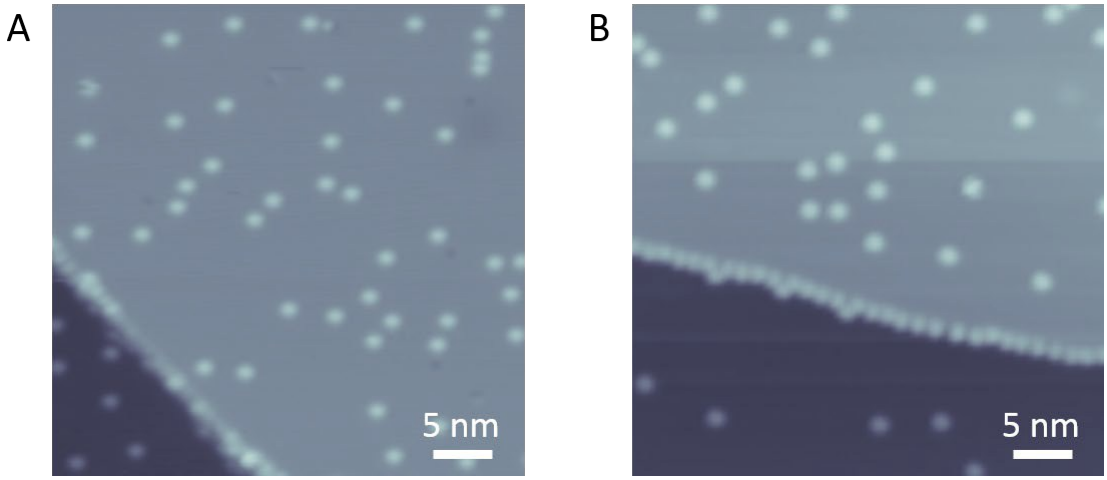

Figure S2. STM images of IMe (A) and IPr (B) deposited on Ag(111) at low temperature. The adsorption of NHCs on pristine Ag(111) surfaces without borophene was initially examined. The deposited NHCs, either IMe or IPr, were found to adsorb onto Ag(111) terraces as isolated single molecules. These observations are in sharp contrast to the previous studies of NHCs on coinage metals deposited at room temperature, where NHCs tend to self-assemble into ordered molecular patterns.[1-3]

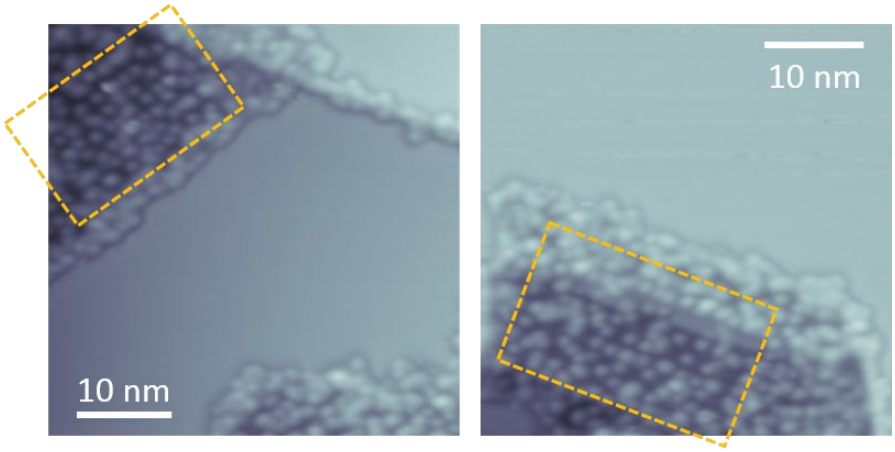

Figure S3. High-coverage IMe molecules on borophene.
Local linear molecular arrangements on borophene are indicated with boxes. STM conditions: (A) 1.5 V, 20 pA; (B) 1.5 V, 35 pA.

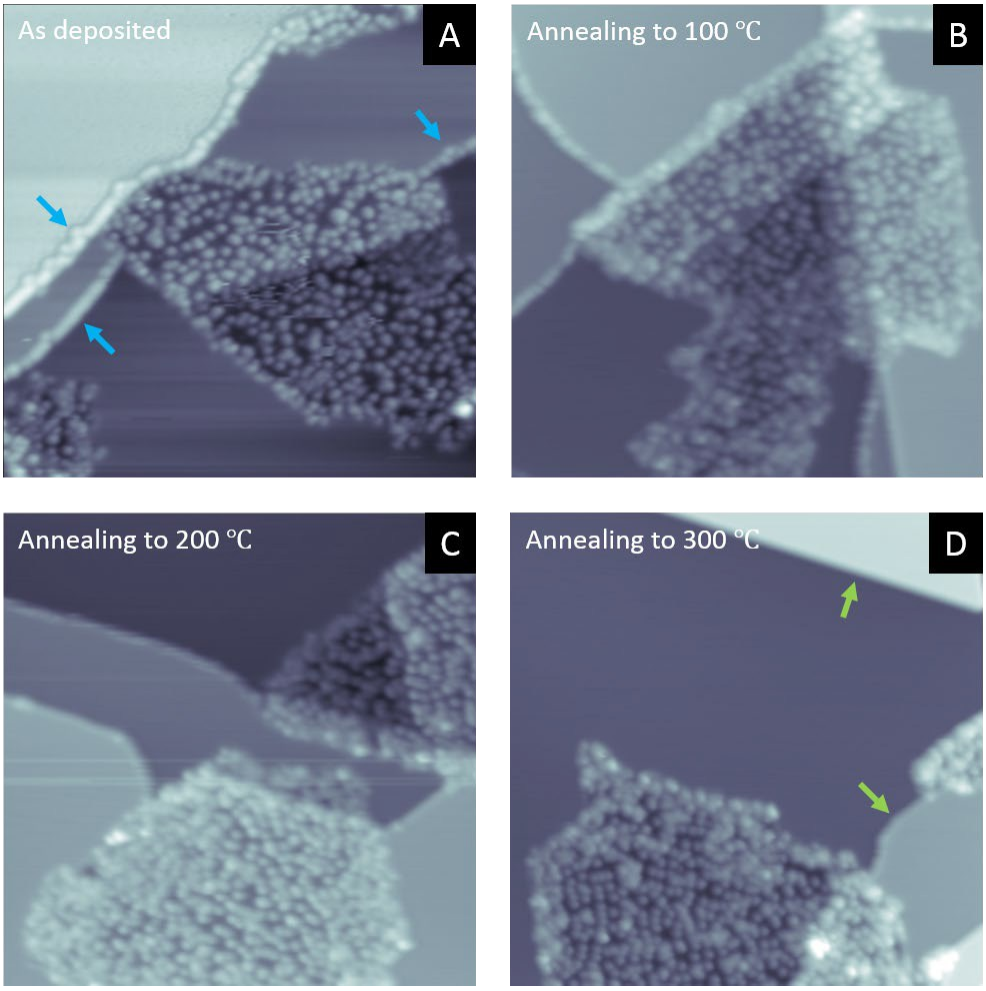

Figure S4. Thermal stability of IMe on borophene.
(A) STM image of as-grown IMe/borophene sample.
(B–D) The same sample after annealing to 100, 200, and 300 ˚C, respectively.
All images are 60 nm × 60 nm in size. STM conditions: (A) 1.0 V, 22 pA; (B) 1.5 V, 20 pA; (C) 1.0 V, 34 pA; (D) 1.5 V, 20 pA.
IMe molecules adsorbed on Ag(111) step edges (blue arrows) are absent (desorbed) after annealing to 300 ˚C (green arrows), while IMe monolayers remain stable on borophene surfaces. These observations suggest a significantly strong interaction of IMe with borophene.

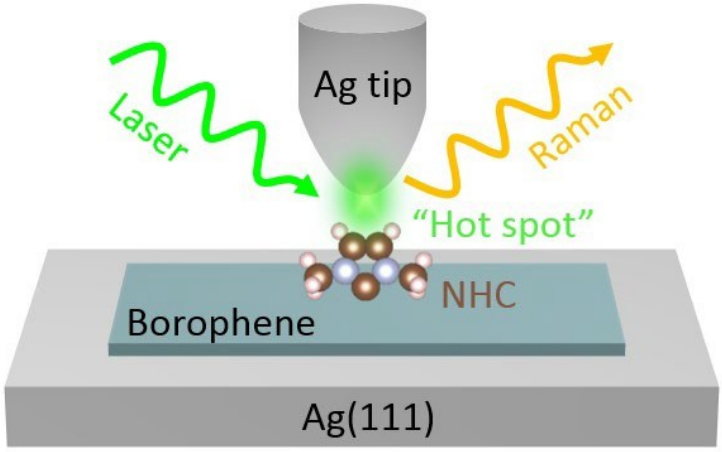

Figure S5. Schematic TERS setup.
"Hot spot" denotes a highly localized region of intense enhanced electromagnetic field, which is generated by surface plasmon resonances of the Ag tip's apex and results in enhanced Raman scattering of nearby molecules.

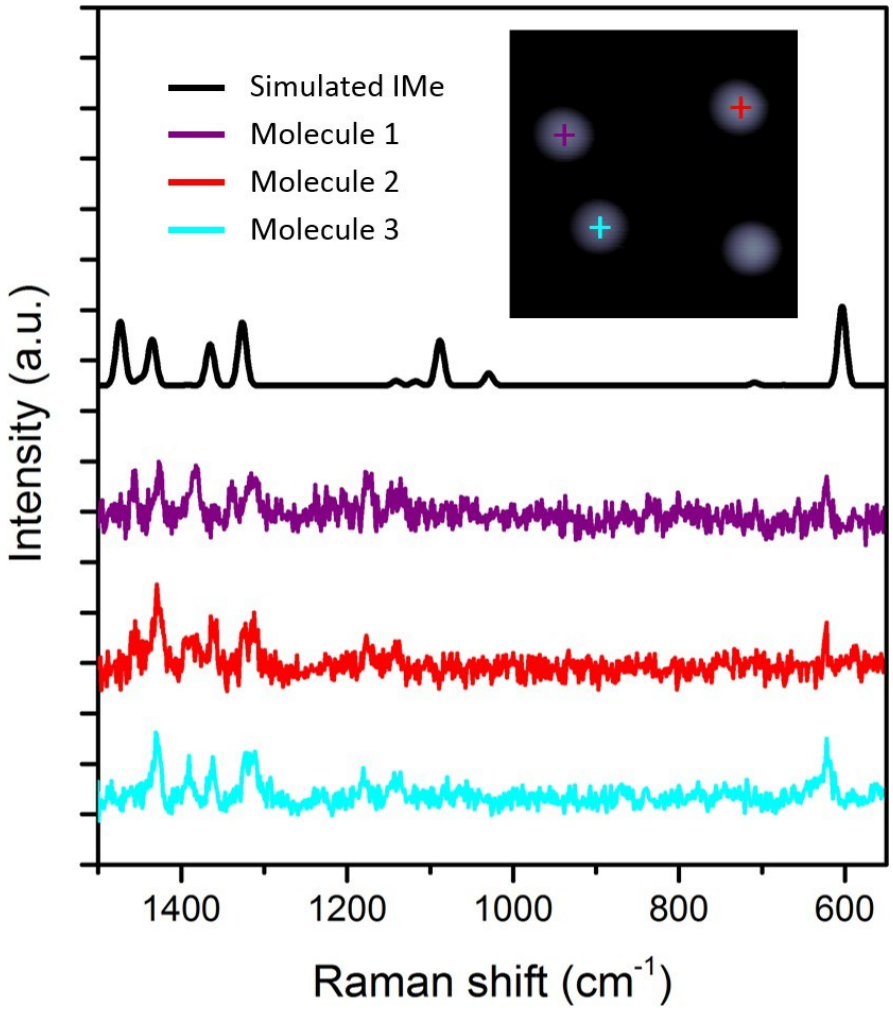

Figure S6. Additional TERS measurements on different single IMe molecules showing similar spectral profiles.

The spectrum in red is the one presented in Figure 2C.

Inset: 7.6 nm × 7.6 nm. STM conditions: 1.0 V, 15 pA. TERS parameters: 0.1 V, 1.0 nA, 5 s.

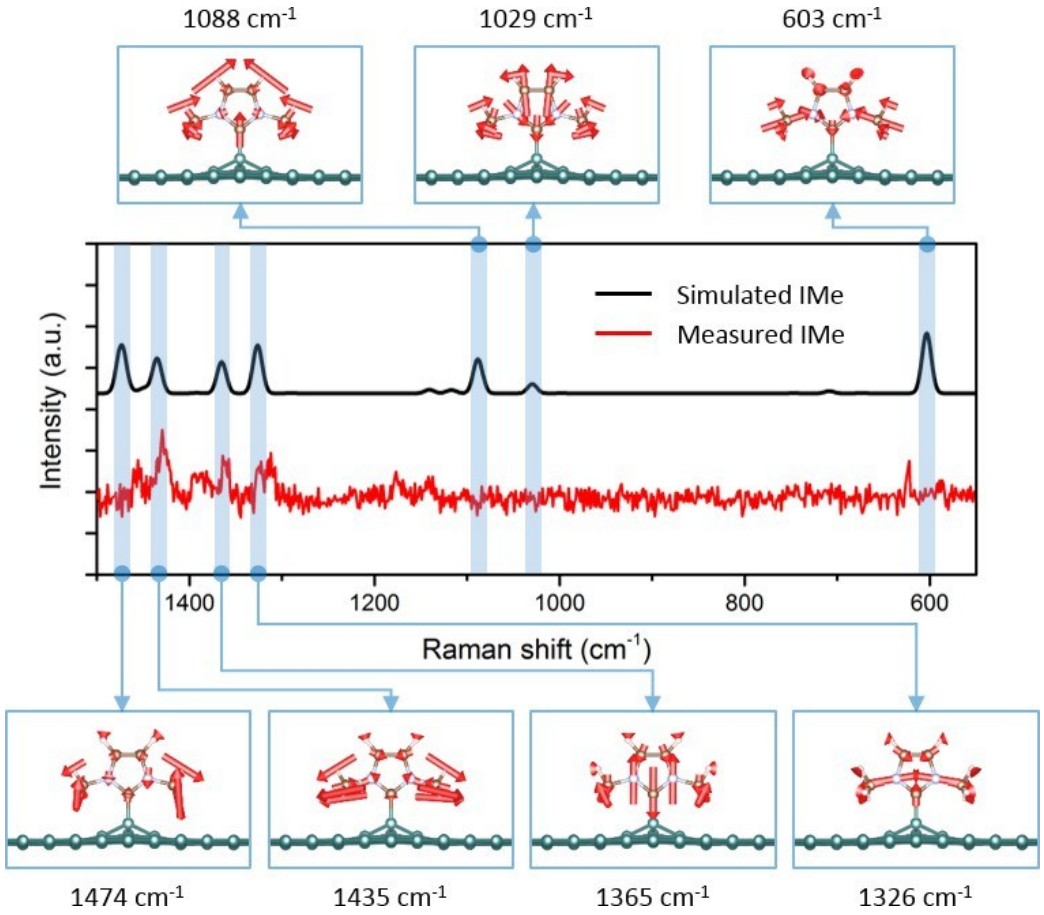

Figure S7. Diagrams of the simulated vibrational modes of IMe on borophene. Consistent with the surface-enhanced Raman spectroscopy (SERS) studies of NHCs on gold surfaces,[4-6] the notable enhanced Raman modes of IMe on borophene are present in the region above 600 cm^{-1}. In particular, the intense bands at 1474 and 1435 cm^{-1} are due to the motion of the hydrogen atoms in the methyl groups. A similar enhancement of Raman modes correlated with the movement of the hydrogen atoms of side groups has been demonstrated in SERS spectra.[5] In addition to these modes centered on the side groups, two intense modes centered on the imidazole ring are observed at 1365 and 1326 cm^{-1}, both of which are dominated by the vibration of nitrogen atoms. It is noteworthy that in SERS spectra the most intense Raman modes exclusively arise from the motion of the hydrogen atoms of side groups, which has been attributed to the proximity of these hydrogen atoms to the surface plasmon.[5] By contrast, additional active Raman modes are visible in TERS spectra, such as those related to the imidazole ring. The difference in the preference of enhanced modes between SERS and TERS can be rationalized by the gap-mode plasmon effect of TERS, which not only allows surface enhancement but also allows additional enhancement from the plasmonically-active tip. This tip–surface doubly enhanced Raman scattering features an extended plasmonic "antenna" normal to the surface, which enables more Raman modes to be enhanced and visible. Remarkably,

although it is elusive to identify a diagnostic peak that corresponds to a primary C–B stretch, an insight provided by Lasse Jensen, Jon P. Camden, David M. Jenkins *et al*.,[7] we note that the 1365 cm^{-1} mode contains considerable carbene carbon contribution, that is, a prominent carbon motion along the B–C bond axis.

Slight mismatches between the calculated and experimental spectra are observed, which could be attributed to the simplified calculation model where the effect from the Ag substrate and Ag tip was not taken into consideration. It has been well demonstrated that significant electron transfer doping occurs for borophene from the Ag(111) substrate, which would have an impact on the vibrational modes of NHC molecules covalently grafted on borophene. In addition to offering a plasmonic “antenna”, the Ag atoms of the tip at the apex may interact with certain electronic orbitals of the molecule in a close affinity, which could promote charge-transfer excitations, influence the electronic structure of the molecule, and thus enhance or shift specific Raman modes. For example, the 1088 and 1029 cm^{-1} modes show discrepancies with the measurement, which are dominated by the movement of the imidazole ring hydrogen and carbon atoms respectively located closest to the tip.

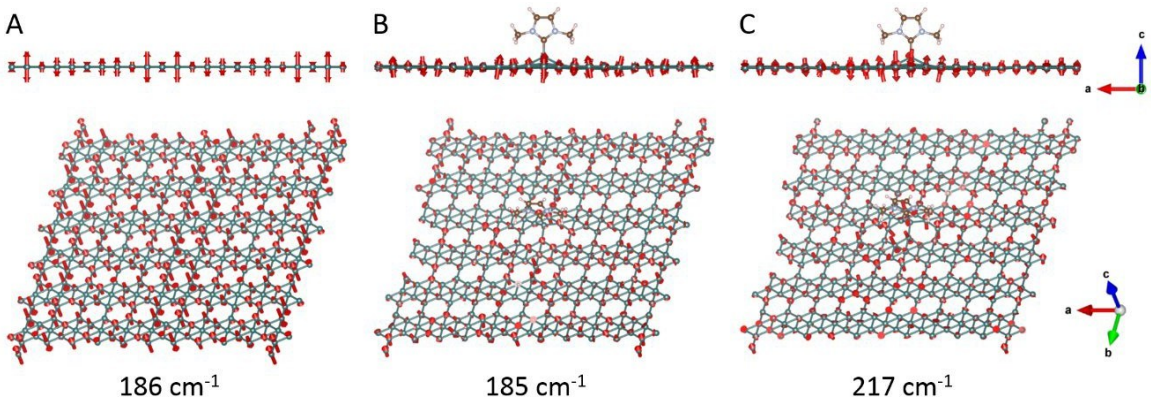

Figure S8. Schematic of the calculated phonon modes of pristine (A) and IMe-modified (B and C) borophene corresponding to the TERS profiles shown in Figure 2D.

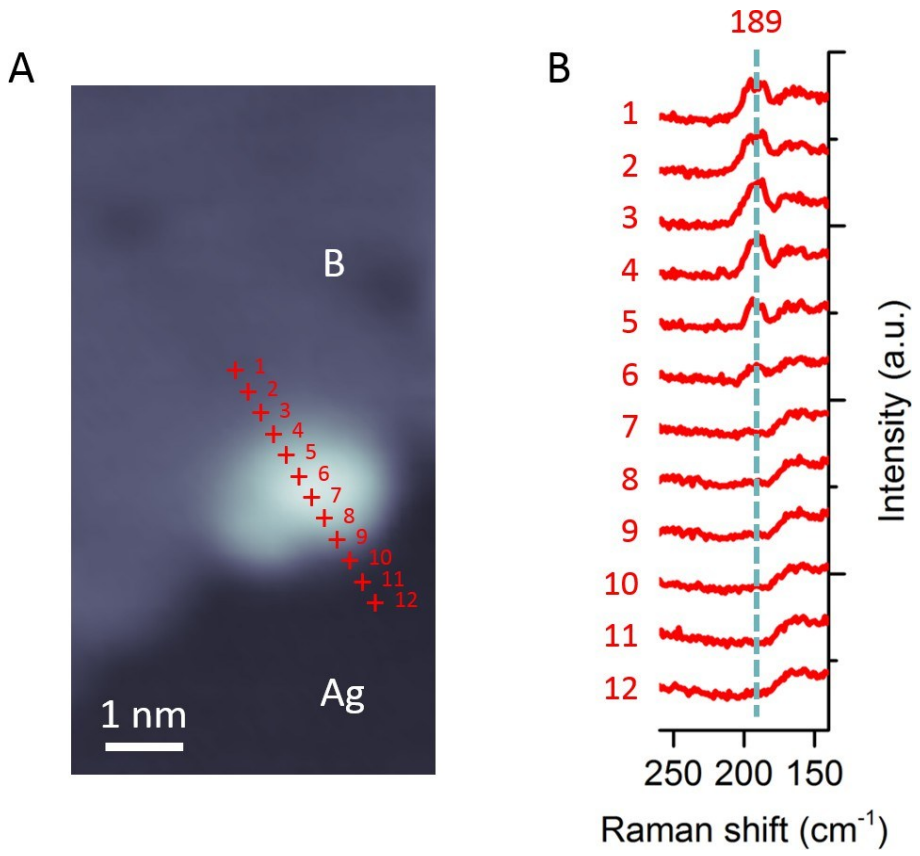

Figure S9. The adsorption of IPr on the edge of borophene.
(A) STM image of a single IPr adsorbed on the edge of a borophene island on Ag(111).
(B) TERS line scan along the tip trace shown in (A).
STM conditions: 3.0 V, 100 pA. TERS parameters: 0.1 V, 1.5 nA, 5 s, with a step length of 3.2 Å.

The chemical nanoenvironments of surface-adsorbed NHC molecules can be determined by sub-nanoscale-resolved TERS measurements. As shown in Figure S9, the vibrational signature of borophene (189 cm^{-1} mode) decreases in intensity and finally vanishes while the tip moves from site 1 to site 12, thereby distinguishing the borophene region from the Ag(111) surface. Particularly over the molecule, the observation of the 189 cm^{-1} peak at sites 4–6 as opposed to the absence of the 189 cm^{-1} peak at sites 7–9 chemically demonstrates that one half (top-left) of the IPr is on top of the borophene island and the other half (bottom-right) is over the Ag(111) surface. That is, the IPr molecule is adsorbed at the borophene–Ag interface.

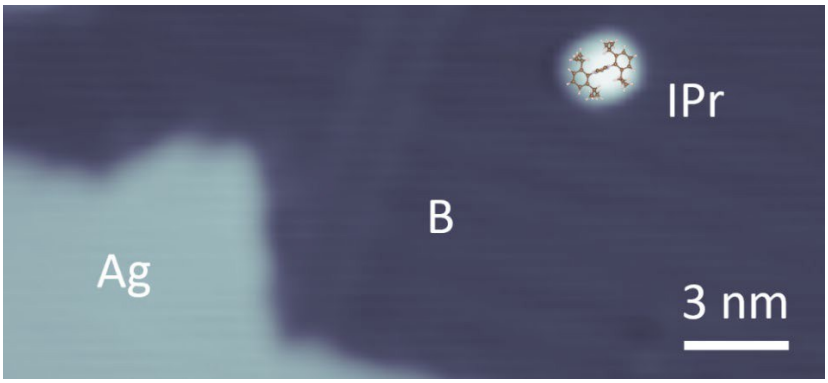

Figure S10. STM image of a single IPr on borophene overlaid with the molecular model (top view).
STM conditions: 1.2 V, 34 pA.

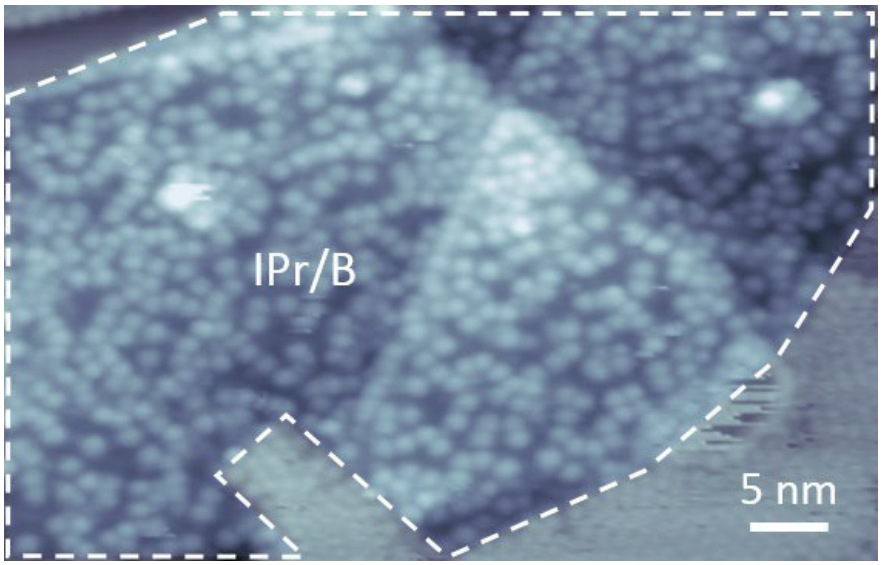

Figure S11. STM topography of IPr on borophene with high coverage.
A borophene region is indicated by dashed lines.
STM conditions: 2.0 V, 210 pA.

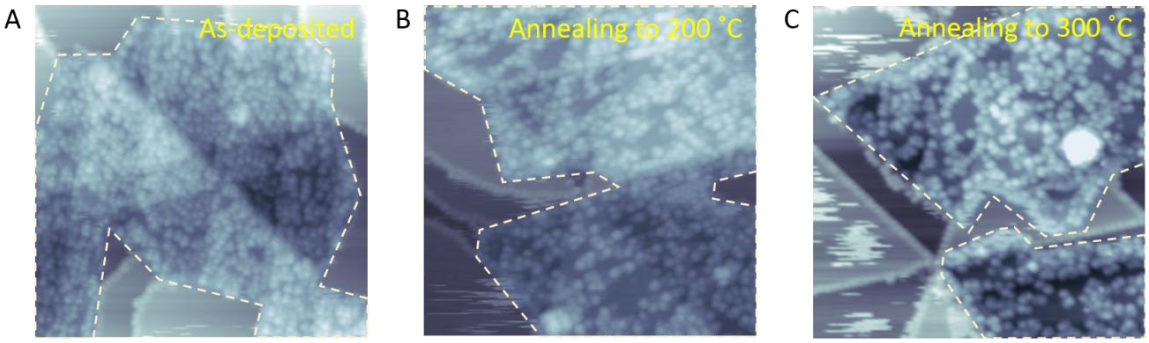

Figure S12. Thermal stability of IPr on borophene.
(A) STM image of as-deposited IPr/borophene sample.
(B) The same sample after annealing at 200 ˚C for 10 min.
(C) The same sample after annealing at 300 ˚C for 10 min.
Borophene regions are indicated by dashed lines. All images are 60 nm × 60 nm in size. STM conditions: (A) -1.5 V, 160 pA; (B) -2 V, 130 pA; (C) -2 V, 85 pA.
After annealing to 200 and 300 ˚C, the size of molecular adsorbates on borophene appeared to increase and the molecular coverage apparently reduced, which indicates clustering and desorption of IPr molecules at elevated temperatures.

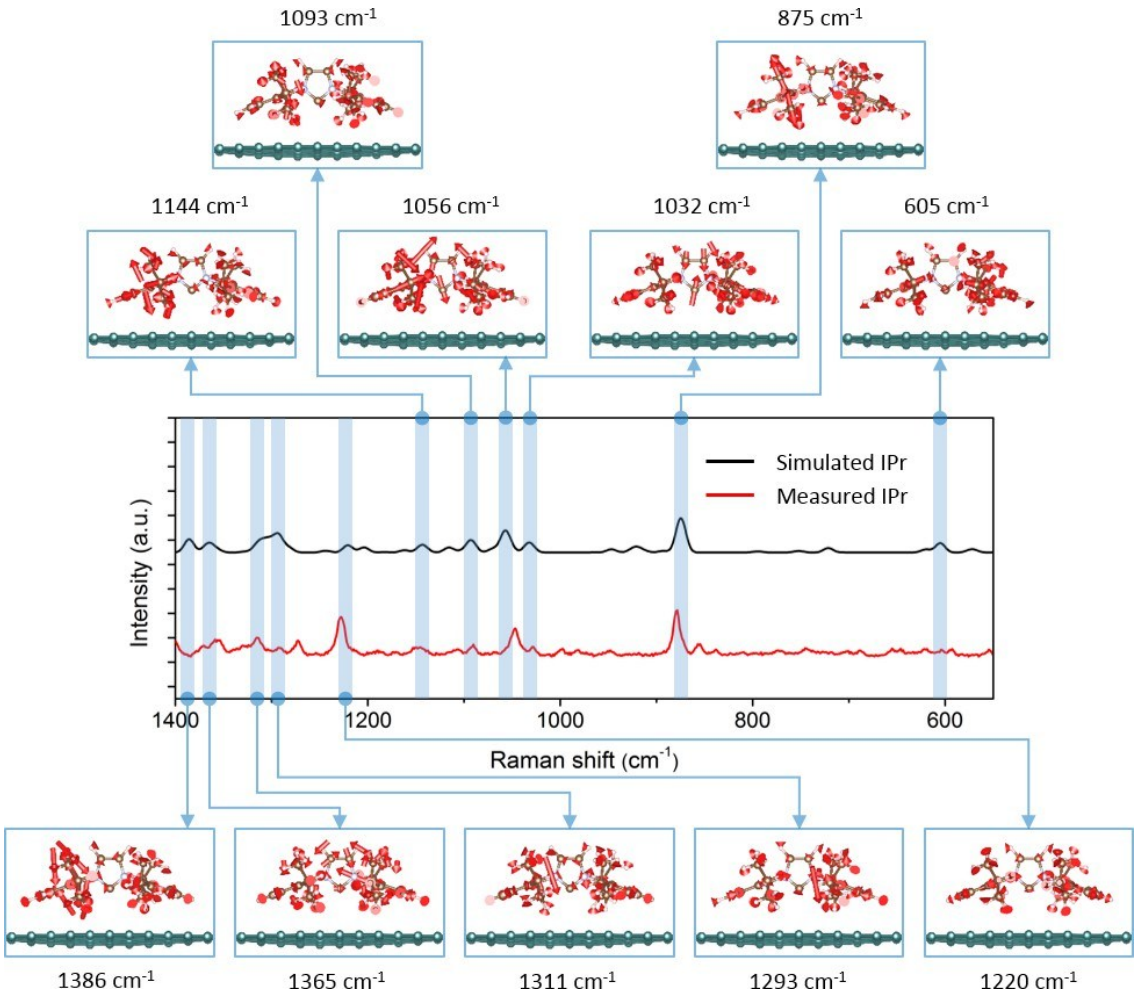

Figure S13. Diagrams of the simulated vibrational modes of IPr on borophene.
Due to the lack of chemisorption of IPr on borophene, the Ag(111) substrate under borophene has limited impact on the chemical properties of IPr despite the strong coupling between borophene and the Ag substrate. Consequently, the measured Raman spectrum can be nicely reproduced by the Raman simulation that did not consider the interplay between borophene and Ag substrate. Nevertheless, very slight distinctions between calculated and measured bands can be visible at 1386, 1293, and 1056 cm^{-1}. We noticed that these modes are due to the motion of the hydrogen atoms of the isopropyl groups bound to the phenyl rings on the N-substituents. As demonstrated in SERS studies of NHCs, SERS (also TERS) spectra are very sensitive to the orientation of the side groups.[5] The four isopropyl groups of IPr most likely have multiple energetically favorable orientations and conformations on borophene while our Raman simulation was based on one of them, which could account for the observed tiny discrepancies. Overall, an excellent agreement between calculated and experimental TERS of IPr on borophene can be identified.

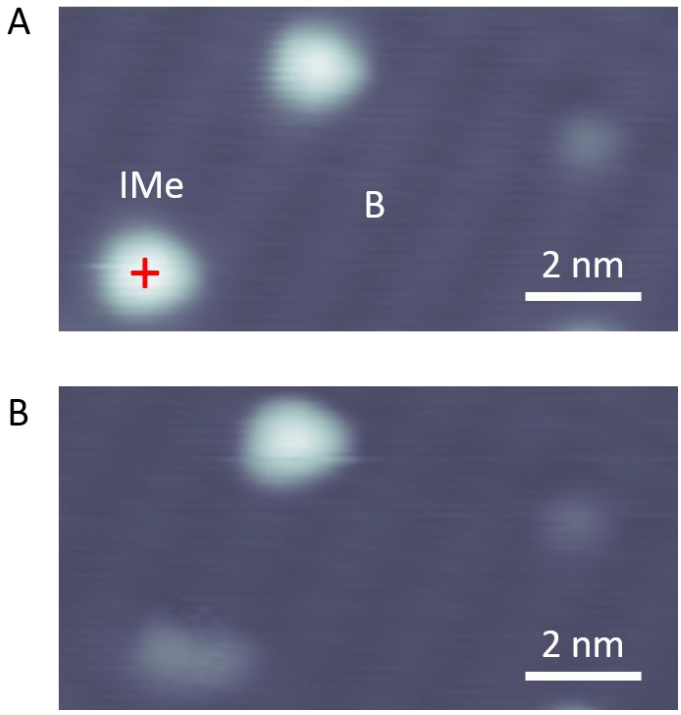

Figure S14. Typical STM images of single IMe molecules on borophene before (A) and after (B) conducting FER spectroscopy with bias voltages above 6 V.
Red plus indicates the tip position for FER measurements. Decomposition, deformation or movement of IMe is observed following FER measurements, suggesting the instability of IMe under local high electric fields.
STM conditions: (A and B) 2.0 V, 30 pA.

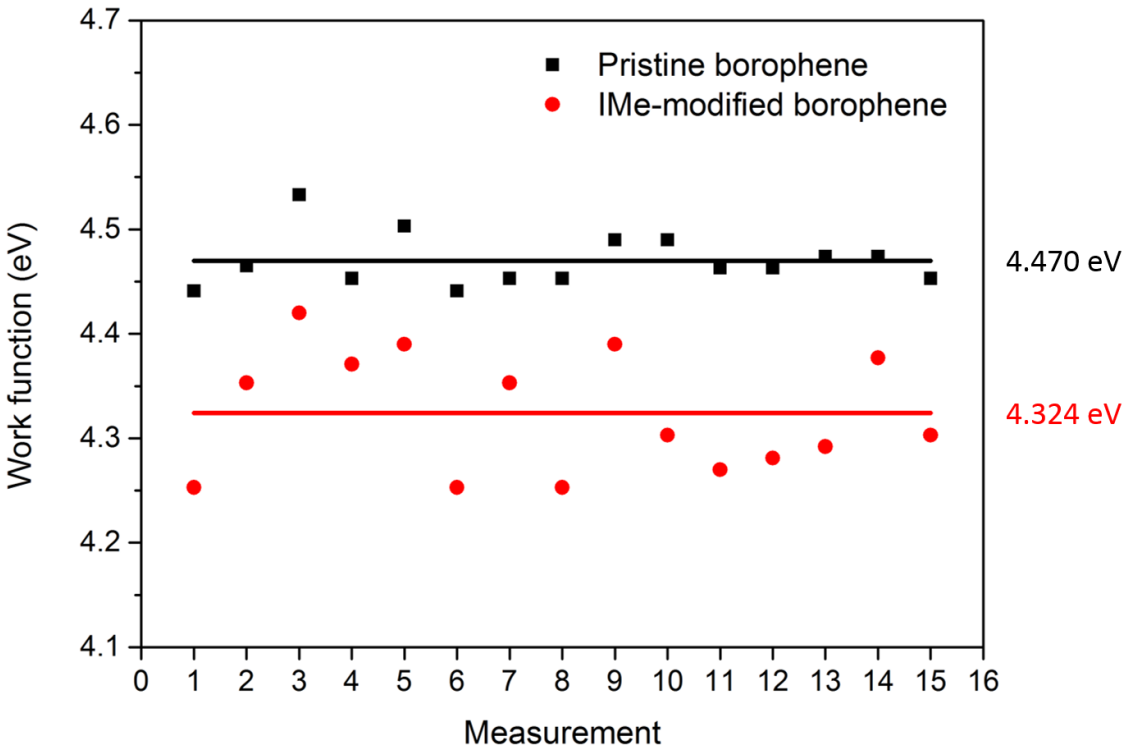

Figure S15. Statistical analysis of work function measurements performed on thirty (fifteen groups) different borophene regions with and without single IMe. Each group of measurements contains FER spectroscopic characterization on pristine borophene (black square) and on single IMe modified borophene (red dot). Statistical analysis results in an average work function reduction of $\Delta\phi_{IMe}^{Exp.}$=0.146 eV due to NHC modification.

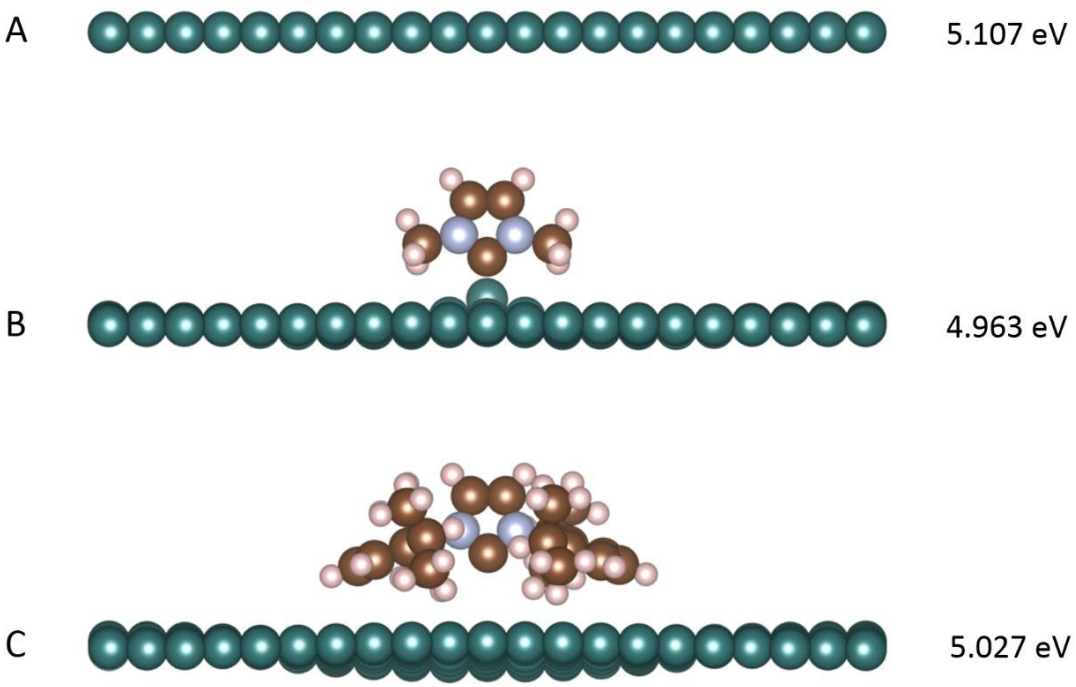

Figure S16. Calculated work functions of pristine borophene (A), locally modified borophene with a single IMe (B), and with a single IPr (C).
Side views for all models.

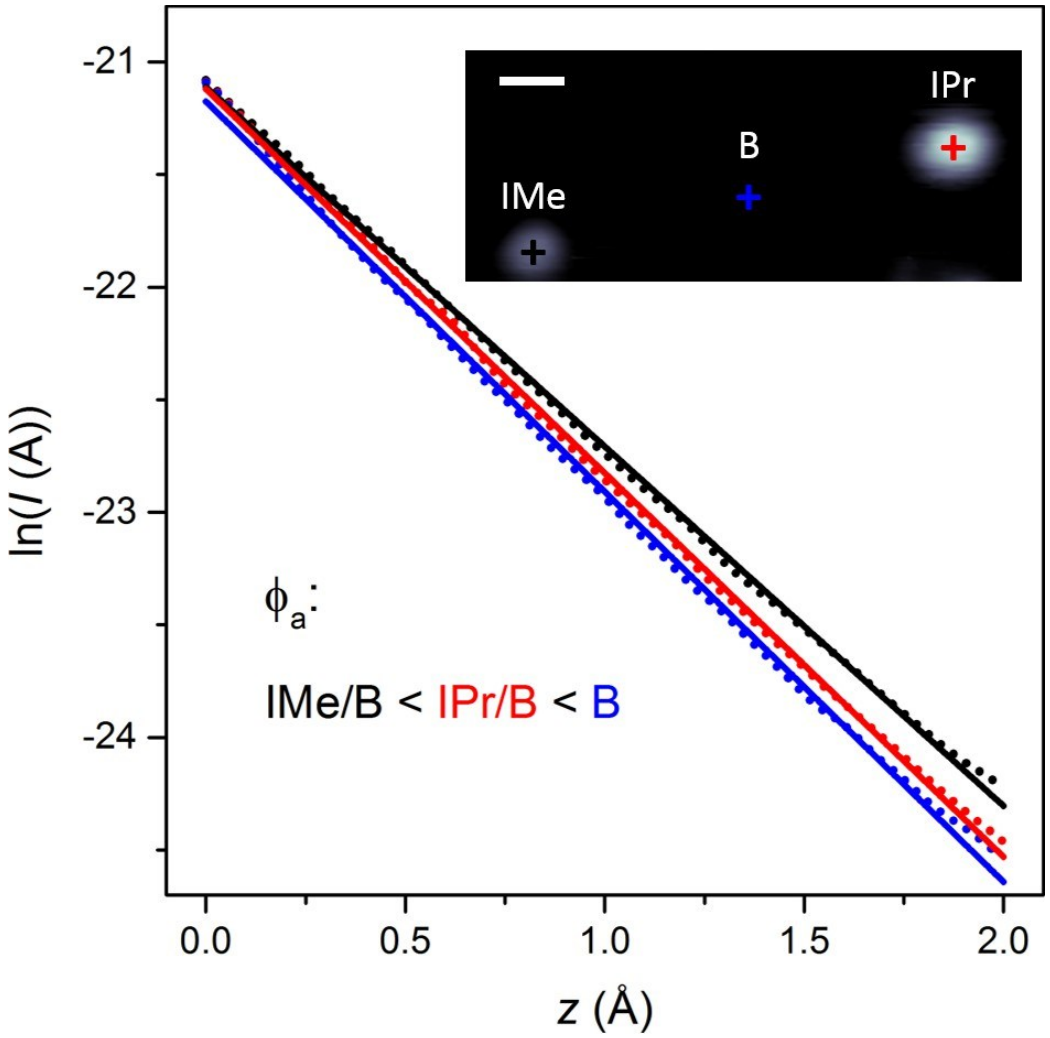

Figure S17. Apparent barrier height (ϕ_a) measurements suggesting a larger work function reduction on IMe-modified borophene compared to IPr-modified borophene. Inset: STM image of single IMe and IPr molecules co-deposited on borophene, where pluses mark the tip positions for STS measurements. Scale bar: 2 nm.
STM conditions: 2.7 V, 30 pA.

Supplemental References

1. Jiang, L., Zhang, B.D., Médard, G., Seitsonen, A.P., Haag, F., Allegretti, F., Reichert, J., Kuster, B., Barth, J.V., and Papageorgiou, A.C. (2017). N-Heterocyclic carbenes on close-packed coinage metal surfaces: bis-carbene metal adatom bonding scheme of monolayer films on Au, Ag and Cu. Chem. Sci. *8*, 8301-8308.
2. Wang, G.Q., Rühling, A., Amirjalayer, S., Knor, M., Ernst, J.B., Richter, C., Gao, H.J., Timmer, A., Gao, H.Y., Doltsinis, N.L., et al. (2017). Ballbot-type motion of N-heterocyclic carbenes on gold surfaces. Nat. Chem. *9*, 152-156.
3. Navarro, J.J., Das, M., Tosoni, S., Landwehr, F., Koy, M., Heyde, M., Pacchioni, G., Glorius, F., and Roldan Cuenya, B. (2022). Growth of N-Heterocyclic Carbene Assemblies on Cu(100) and Cu(111): From Single Molecules to Magic-Number Islands. Angew. Chem. Int. Ed. *61*, e202202127.
4. DeJesus, J.F., Trujillo, M.J., Camden, J.P., and Jenkins, D.M. (2018). N-Heterocyclic Carbenes as a Robust Platform for Surface-Enhanced Raman Spectroscopy. J. Am. Chem. Soc. *140*, 1247-1250.
5. Trujillo, M.J., Strausser, S.L., Becca, J.C., DeJesus, J.F., Jensen, L., Jenkins, D.M., and Camden, J.P. (2018). Using SERS To Understand the Binding of N-Heterocyclic Carbenes to Gold Surfaces. J. Phys. Chem. Lett. *9*, 6779-6785.
6. Thimes, R.L., Santos, A.V.B., Chen, R., Kaur, G., Jensen, L., Jenkins, D.M., and Camden, J.P. (2023). Using Surface-Enhanced Raman Spectroscopy to Unravel the Wingtip-Dependent Orientation of N-Heterocyclic Carbenes on Gold Nanoparticles. J. Phys. Chem. Lett. *14*, 4219-4224.
7. Jensen, I.M., Chowdhury, S., Hu, G.H., Jensen, L., Camden, J.P., and Jenkins, D.M. (2023). Seeking a Au–C stretch on gold nanoparticles with ^{13}C-labeled N-heterocyclic carbenes. Chem. Commun. *59*, 14524-14527.